J Solid State Electrochem (2011) 15:23–46
DOI 10.1007/s10008-010-1123-8

REVIEW

Fundamental and applied electrochemistry at an industrial glass laboratory—an overview

Friedrich G. K. Baucke

Received: 18 May 2010 / Revised: 1 June 2010 / Accepted: 4 June 2010 / Published online: 24 August 2010

Abstract This paper is a review of the author's work at the SCHOTT Electrochemical Laboratory from 1965 to 1995. Special emphasis is given to the elucidation of the functioning of the glass electrode, mobility of cations in glasses, and to the research on the electrochemistry of glass melts.

Keywords Glass electrode · pH · pD · Reaction mechanism · Redox · Conductivity · Seebeck effect

Introduction

When the author of this paper had returned from his job as postdoctoral fellow at the University of California, Berkeley, to Germany in 1965, he joined the Jena^{er} Glaswerk, later SCHOTT Glaswerke, now SCHOTT AG, where he was asked to found a laboratory especially designed for electrochemical work. Besides the glass electrode, a SCHOTT product, whose functioning was completely unclear at that time, only few electrochemical problems to be treated in the near future could be anticipated. Nevertheless, the company agreed that an Electrochemical Laboratory was founded, and indeed, it remained the only laboratory of its kind within the glass industry for many tens of years. The elucidation of the glass electrode mechanism, the most extensive work, did not remain the only problem to be solved in the future, but many other tasks came up. For example, there was the related problem of understanding the functioning of the glass electrode in heavy water solutions, i.e., the measurement of pD and pM(D_2O) values, the question of accurately determining thermoelectric voltages in molten glasses, the construction of a conductivity cell for glass melts up to 2,000°C or above, the investigation of the interaction of glass melts with ceramic materials applied for constructing glass melters, redox problems of glass melts, which are the basis of redox fining, and the deleterious formation of oxygen bubbles in glass melts. In addition, thin layer systems with continuously changeable reflectivity for automotive rear view mirrors were developed as a completely new kind of product.

It may surprise at first sight that the Electrochemical Laboratory, an industrial laboratory, was involved also in fundamental glass research. However, this is not surprising when the nature of most of the problems to be treated is considered. It reflects the author's conviction that also tasks done at the industry, although primarily aimed at practical solutions, can be solved only by understanding the basic chemical and electrochemical problems involved. This fact resulted in a relatively large number of fundamental investigations in addition to the practical work done. In several cases, the work was even carried beyond the envisaged solution because of the author's scientific interests and yielded additional fundamental information, which repeatedly proved to be significant for further work to be done.

This paper then presents examples of the work carried out at SCHOTT Electrochemical Laboratory from 1965 to 1995. Some of them were chosen because they describe specifically developed techniques for solving special problems, others because they report on new scientific results. The entire work can be found in a book [1], which should be consulted for more details if required.

Friedrich G. K. Baucke was formerly affiliated with SCHOTT AG, Mainz, Germany.

F. G. K. Baucke (✉)
Kaiserstraße 36,
55116 Mainz, Germany
e-mail: f-baucke@t-online.de

Glass electrodes

General The functioning of glass electrodes is based on a potential difference between two electrolytes, a solid (glass) and a liquid electrolyte (solution), and thus differs basically from metal–metal and redox electrodes. The metal contacts of the glass electrode cell are accomplished by extending the two-phase system glass/electrolyte solution by additional phases so that the system becomes a galvanic cell with two metal terminals. The interesting fundamental question is then the mechanism by which the potential difference between glass membrane and solution is formed.

Hypotheses of potential formation When the Electrochemical Laboratory was founded in 1965, there existed over 30 different theories (or hypotheses) of the potential formation between the two electrolytes [2]. Examples were the "water-phase theory" [3], the first theory developed by Haber in 1909 [4], who also constructed the first glass electrode and applied it for acidimetric titrations. Many other theories based on different physical and chemical phenomena followed, for instance, the adsorption theory by Lengyel (1931) [5], a theory by Cremer (1924) based on an assumed permeability of glasses to hydrogen ions [6], a strange assumption, also because Cremer had detected the "glass electrode effect," i.e., the potential difference between a solid and a liquid electrolyte, during his search for a semipermeable membrane in 1906 [7] and is thus often called the inventor of the glass electrode. There are many names and many ideas which, in addition, are often mixed and thus increase the number of hypotheses. The advent of radioactive tracers in the 1950s [8] did not yield any more insight, and even in 1964, Schwabe and Suschke refereed on four simultaneously existing theories [8].

The longest lived hypothesis was Nicolsky's ion exchange theory (1937) [9], which he based on Schiller's (1924) [10] and Horowitz' and Zimmermann's (1925) [11] idea of an exchange of different ions between glass and solution. The ion exchange theory was strongly supported by Eisenman, who also combined it with results of his radiotracer experiments in the 1960s [12]. Based on purely thermodynamic arguments and relatively correct experimental results obtained by Nicolsky's equation, the ion exchange theory was soon strongly believed to represent the real physical process of the glass electrode function. This conclusion triggered a tremendous amount of theoretical and experimental work by which the researchers tried to do the impossible, i.e., to refine a non-existent mechanism by means of assuming more mechanistic details in order to fit the thermodynamic Nicolsky equation to the experiments. During these about 30 years, any new ideas were nearly excluded, and the development of the glass electrode was hindered or even stopped [13]. It is highly surprising that none of the many scientists involved had the correct idea, i.e., that thermodynamics can basically neither explain nor exclude any reaction mechanism. What was missing was any knowledge about the ionic processes at the phase boundary glass/solution and in the surface range of the glass.

Modern analytical methods The situation changed in the early 1970s when H. Bach of SCHOTT AG published a method for measuring continuous concentration profiles in subsurface glass layers by means of ion ablating the glass with monoenergetic argon ions and simultaneous recording the intensity of characteristic spectral lines of the elements of interest [14]. Due to its sensitivity and the extreme depth resolution of 3 to 5 nm, the technique is well suited to investigate processes at and below electrode glass surfaces. In addition, rather short analysis times, i.e., in the range of an hour or less per concentration profile, are needed. All of the properties of this technique called *ion bombardment for spectrochemical analysis* (IBSCA) are also extremely favorable compared to Boksay's first ingenious method [15] of measuring concentration profiles by layerwise dissolution of the glass with a glass-dissolving solution ($HF+H_2SO_4$) and a quantitative analysis of the solution fractions (1964). IBSCA was exactly the tool that had been missing during the unsuccessful 30 years of thermodynamic investigations, as it yielded data necessary also to make other methods applicable to the reactions at and below glass surfaces. It was thus combined with electrochemical and non-electrochemical methods, for instance, with coulometry, spectroscopy, electrolysis, and potentiometry, to membrane glasses before and after contact with electrolyte solutions in order to investigate so-called glass leaching and as an indicating method after electrolyzing samples of certain glasses for various periods to study field-driven ionic migration within the solids. The latter application presents a modification of the well-known *moving boundary method* (MBM) applied to electrolyses in electrolyte solutions [16]. The *modified moving boundary method* (mMBM) yields even more information than the basic technique MBM, as it reveals not only the distance of the concentration "steps" from the glass surface but also their concentration profiles and their development during the migration processes (see [1], p. 140ff). In several cases, the results obtained by IBSCA are confirmed by a related method called *nuclear reaction analysis* (NRA; see [1], p. 56). This is of particular interest for hydrogen concentration profiles in glasses, which are not directly measurable by IBSCA but must be obtained as profile differences of other elements.

The electrode mechanism The described modern analytical techniques have shown that the glass electrode

response is the consequence of an interfacial equilibrium between functional groups R, e.g., ≡SiO or [≡AlOSi≡] at the immediate glass surface (s) and thus in contact with the solution, and hydronium (H_3O^+) and/or alkali (M^+) ions in the solution (soln) [17]. Depending on glass composition, i.e., relative pH and pM, the surface is covered at equilibrium with the neutral acid (RH) and/or the salt form (RM) of the groups at the glass surface and contains a minute concentration of the anionic, negatively charged component R^- resulting from the dissociation of one or both of the neutral groups. The anionic groups represent a negative charge density at the glass surface and thus a negative potential of the glass membrane relative to that of the solution. The potential difference ε_m between glass and solution consequently is a quantitative function of the solution pH and/or pM, $\varepsilon_m = f(\mathrm{pH}, \mathrm{pM})$. This dependence is the key to understanding the functioning of the glass electrode and is called *dissociation mechanism*, which we mentioned in the literature for the first time in 1974 [18] and in 1975 [19].

Dissociation and association of the neutral glass surface groups are thermodynamically described by their equilibria, which are coupled by the common negative surface group R^-, Eq. 1a,

$$\mathrm{RH(s)} + \mathrm{H_2O(soln)} \rightleftarrows \mathrm{R^-(s)} + \mathrm{H_3O^+(soln)};\ K''_{\mathrm{D,H}} \tag{1a}$$

and Eq. 1b,

$$\mathrm{R^-(s)} + \mathrm{M^+(soln)} \rightleftarrows \mathrm{RM(s)};\ K'_{\mathrm{A,M}}. \tag{1b}$$

However, Eqs. 1a and 1b can be advantageously combined to form the "crossed" or "combined equilibria," Eq. 1,

$$\begin{array}{c} \mathrm{M^+(soln)} \\ + \\ \mathrm{RH(s)} + \mathrm{H_2O(soln)} \rightleftarrows \mathrm{R^-(s)} + \mathrm{H_3O^+(soln)} \\ \uparrow\downarrow \\ \mathrm{RM(s)}, \end{array} \tag{1}$$

which shows more clearly that the anionic form of the surface groups links the equilibria, Eqs. 1a and 1b, whereas it cancels if Eq. 1a is added to Eq. 1b so that the important term, $R^-(s)$, which determines the sign of the glass surface, is missing and the treatment is meaningless.

The single equilibrium constants $K'_{\mathrm{D,H}}$ and $K''_{\mathrm{A,M}}$ of the *dissociation mechanism* have extremely different magnitudes so that in most cases, only one of the equilibria of Eq. 1, determines the actual situation. Thus, either the acid dissociation equilibrium, Eq. 1a, or the salt association equilibrium, Eq. 1b, may determine the immediate function of the glass electrode, whereas within the transition region between these ranges, which spans approximately ΔpH or ΔpM=±2, the functioning is determined by both equilibria simultaneously and is characterized by the selectivity product $\left(K'_{\mathrm{D,H}}K''_{\mathrm{A,M}}\right)$ (see [1], p. 86), the magnitude of which can easily be determined, whereas the heterogeneous single equilibrium constants are not directly measurable. However, we estimated correlated relative couples of $K'_{\mathrm{D,H}}$ and $K''_{\mathrm{A,M}}$ of several electrode glasses (see [1], p. 87). For example, for a lithium silicate pH glass, the correlated constants were found to be $K'_{\mathrm{D,H}} \leq 10^{-16}$ mol kg^{-1} and $K''_{\mathrm{A,Li}} \geq 10^4$ kg mol^{-1}, which yield the selectivity product $\left(K'_{\mathrm{D,H}}K''_{\mathrm{A,Li}}\right) = 10^{-12}$ of the correct order of magnitude for this glass.

The ion exchange theory, on the contrary, treats an ion exchange, as only one equilibrium of cations, Eq. 2 (see [1], p. 50ff),

$$\mathrm{Na^+(glass)} + \mathrm{H_3O^+(soln)} \rightleftarrows \mathrm{H^+(glass)} + \mathrm{Na^+(soln)} + \mathrm{H_2O(soln)}, \tag{2}$$

excludes thus the possibility of a (negative) sign of the glass and does not allow for single equilibrium constants as those for Eq. 1a and Eq. 1b. In addition, the existence of only one equilibrium constant, i.e., the ion exchange constant K_{exch}, Eq. 3,

$$K_{\mathrm{exch}} = \frac{a_{\mathrm{H^+,glass}}\, a_{\mathrm{Na^+,soln}}\, a_{\mathrm{H_2O,soln}}}{a_{\mathrm{Na^+,glass}}\, a_{\mathrm{H_3O^+,soln}}}, \tag{3}$$

does not yield any further insights into the electrode mechanism.

The potential difference of the dissociation mechanism is derived in the usual way from the electrochemical free energy change, which is zero at equilibrium. The pH-dependent potential difference $\varepsilon_{\mathrm{m}} = \varphi_{\mathrm{glass}} - \varphi_{\mathrm{solution}}$, for example, results as Eq. 4,

$$\varepsilon_{\mathrm{m}} = -k \log K''_{\mathrm{D,H}} + \log \frac{a'_{\mathrm{R^-}}}{a'_{\mathrm{RH}} a_{\mathrm{H_2O}}} - k\mathrm{pH}, \tag{4}$$

and shows the usually observed dependence of the linear potential difference on pH. k=2.303RT/F is the Nernst slope, a is the activity of dissolved species, and a' is that of surface groups. The dependence of the potential difference on pM (M=alkali) is obtained in a corresponding way and that on both pH and pM, i.e., in the transition range, in a similar way, however, by observing that the total surface concentration consists of the sum of all concentrations of acidic, salt, and anionic groups, $\sum c' = c'_{\mathrm{RH}} + c'_{\mathrm{RM}} + c'_{\mathrm{R^-}}$.

The number of *hydrogen ions released by the dissociation of the surface SiOH groups*, Eq. 1a, incidentally, although added to the number of hydrogen ions in the solution, is equal to the minute number of dissociating anionic surface groups and does not change the pH of the solution in any detectable way [20]. In this sense, glass electrodes are ideally inert sensors.

Heterogeneous single equilibrium constants Different from homogeneous equilibrium constants, the magnitude of heterogeneous equilibrium constants, Eqs. 1a and 1b, is not only determined by the chemical driving force of dissociation/association but also by the coulombic force between the negatively charged glass surface and the positive charge of the dissociated (released) cations [21]. This leads to equilibrium constants, which are given by a compromise of the counteracting forces. Heterogeneous dissociation/association constants are thus much smaller/larger than they would be if the surface groups were dissolved as single molecules (see the estimated correlated relative couples of $K'_{D,H}$ and $K'_{A,M}$ above). Also, the negative surface charge of the glass results in the formation of salt groups with alkali ions, for example, SiONa, although alkali salts are usually nearly completely dissociated in aqueous solutions. These surface groups cause the alkali error in light and heavy water solutions and thus present an onset of the alkali sensitivity of silicate membrane glasses. Alkali-sensitive membrane glasses, on the contrary, contain various contents of aluminosilicate and will be discussed at a later occasion.

Explanation of sub-ideal (sub-Nernstian) response of glass electrodes It is usually assumed that glass electrodes exhibit the "ideal slope" $k = 2.303RT/F$ or Nernstian response of their potential [21]. However, it has been reported that the response can also be sub-Nernstian, i.e., that the slope can be below (but never above) k. The cause of this "electrode error" is that the equation yielding the potential difference, Eq. 4, is an equilibrium and that a change of the pH is necessarily coupled with a counter change of other participants in the equilibrium [22]. In Eq. 4, this is essentially the activity of the anionic surface group, whereas neutral acid and water activities are practically constant. Since the term $\mathrm{d}\log a'_{R^-}/\mathrm{dpH}$, a positive number, is subtracted from the "ideal slope" k, the thermodynamically correct slope is basically slightly smaller than the ideal slope, Eq. 5,

$$\frac{\mathrm{d}\varepsilon_m}{\mathrm{dpH}} = -\left[1 - \frac{\mathrm{d}}{\mathrm{dpH}}\left(\log\frac{a'_{R^-}}{a'_{RH}a_{H_2O}}\right)\right]k. \tag{5}$$

The rigorous thermodynamically correct expression for the pH-dependent glass electrode potential thus differs from Eq. 4 [22], Eq. 6,

$$\varepsilon_m = \varepsilon^0_H - \left(1 - \frac{\mathrm{d}\log a'_{R^-}}{\mathrm{dpH}}\right)k\mathrm{pH}, \tag{6}$$

where ε^0_H is the standard potential at 100% pH response, and the expression

$$\left(1 - \frac{\mathrm{d}\log a'_{R^-}}{\mathrm{dpH}}\right)k$$

is called "sub-ideal response." It explains the experimental "sub-Nernstian response" αk thermodynamically, the magnitude of which is in the range (0.999 to 0.995)k. It was first reported by Bates, who termed α "electromotive efficiency" [23], Eq. 7,

$$\varepsilon_m = \varepsilon^0_H - \alpha k\mathrm{pH}, \tag{7}$$

which had remained unexplained until its thermodynamic meaning was explained by the work done at Schott Electrochemical Laboratory. (Bates, incidentally, used initially the term β_e instead of α.) We have also discovered that the difference of α with respect to unity, which we call "electromotive loss factor," Eq. 8,

$$n = 1 - \alpha = \frac{\mathrm{d}\log a'_{R^-}}{\mathrm{dpH}}, \tag{8}$$

is more useful because it yields detailed information about the heterogeneous equilibrium and further details of the glass electrode response, although (or because) it is an extremely small number, n=0.001 to 0.005, mean value=0.0025±0.0013 [24]. The electromotive efficiency of, e.g., Schott glass N1120, incidentally, was verified by means of precise potential measurements under various conditions (three individual glass electrodes, two reference electrodes of different types (Thalamid and hydrogen), three standard buffer solutions, and two temperatures, 25°C and 50°C) at Schott laboratory and was found to be temperature-independent within the limits of error, 0.9976 ± 0.0005 (25 °C) and 0.9972 ± 0.0008 (50 °C) [25].

Significance of the electromotive loss factor The minute electromotive loss factor, which we nearly overlooked at first, provides significant information about the interfacial equilibrium between glass and solution. Thus, the practical overall electrode slope, Eq. 9,

$$\frac{\mathrm{d}\varepsilon_m}{\mathrm{dpH}} = -\alpha k = 58.0 \text{ to } 59.1\ \mathrm{mV}\ (25\ ^\circ\mathrm{C}), \tag{9}$$

was split into two terms [17], Eq. 10,

$$\frac{d\varepsilon_m}{\mathrm{dpH}} = \left(\frac{d\varepsilon_m}{\mathrm{d}\log a'_{R^-}}\right)\left(\frac{\mathrm{d}\log a'_{R^-}}{\mathrm{dpH}}\right), \tag{10}$$

the potential difference as a function of the log of the charge density at the glass surface (first brackets on the right side of Eq. 10) and the log of the charge density as a function of the solution composition (second brackets). Since thus, in addition to the overall electrode slope, Eq. 9, also the second term on the right side of Eq. 10 is known, the first term is given by Eq. 11,

$$\frac{\mathrm{d}\varepsilon_m}{\mathrm{d}\log a_{R^-}} = -\frac{(1-n)k}{n} = -\frac{\alpha k}{1-\alpha}, \tag{11}$$

and has the surprising magnitude −11.8 to −59.1 V (!) depending on α [17].

The electromotive loss factor n, Eq. 8, thus provides insight into the practical electrode slope, Eq. 10: (1) The second brackets of Eq. 10 represent a chemical equilibrium, the minute quantity (0.0025) of which may be understood because of dimensional reasons—it is the dependence of the log of a surface concentration, a small number, on pH, a volume concentration, that is larger by orders of magnitude. (2) The first brackets of Eq. 10 represent the charge of the surface groups and thus the potential ε_m of the negative glass surface as a function of the activity (concentration) of the surface groups, which is a physically given number, that is surprisingly large. In short, the free variable pH determines the dependent variable ε_m via a chemical equilibrium and the physically fixed magnitude of its charge.

The "electrochemical structure" of the glass membrane surface The electrochemical state of the membrane surface of glass electrodes has long been a matter of discussion. The questions asked have essentially been (1) "How does the electrochemical structure of the glass surface change with the solution pH and/or pM it indicates?" and (2) "What causes the selectivity of the glass membrane?"

Indeed, answers to these questions could only be given after the mechanism of the electrode functioning had been elucidated [26]: The glass surface is covered with neutral surface groups containing either protons, RH, alkali ions, RM, or both at equilibrium with the contacting solution, Eq. 12,

$$x'_{RM} = 1 - x'_{RH} = \left[\frac{1}{K''_{D,H}K'_{A,M}}\left(\frac{a_{H_3O^+}}{a_{M^+}}\right) + 1\right]^{-1}, \qquad (12)$$

which is based on the selectivity product, $\left(K''_{D,H}K'_{A,M}\right)$. x' is the surface mole fraction of the group indicated. Independent of the coverage according to Eq. 12, the surface groups RH and/or RM dissociate minutely according to their relative concentrations and the crossed equilibrium, Eq. 1, thus yielding the appropriate minute concentrations of charged surface groups R^- and the connected potential ε_m of the glass surface. In other words, the glass surface is characterized by two coupled equilibria: (1) by the surface coverage with neutral groups RH and/or RM according to Eq. 12 providing the releasable cations H^+ and/or M^+ and being thus responsible for the *selectivity* and (2) by the pH- and/or pM-dependent equilibrium, Eq. 1, yielding the potential ε_m according to the single equilibrium constants $K''_{D,H}$ and/or $K'_{A,M}$ and thus yielding the *potential formation*. A major change of the surface coverage proceeds only within a span of about $\Delta pH \leq \pm 4$, i.e., within the transition range, where RH groups at the glass surface replace RM groups or vice versa, Eq. 12.

Interrelation of anionic surface groups and pH The electromotive loss factor n also couples changes of pH values with their origin, the changes of anionic surface groups [17]. Thus, the application of the rearranged version of the electromotive loss factor, Eq. 8, $d \log a_{R^-} = n d\mathrm{pH}$, to two couples of data, for example, to $a'_{R^-,1}$ and pH_1 and to $a'_{R^-,2}$ and pH_2, yields the relative activities of the charged surface groups from the relative pH values, Eq. 13,

$$\log \frac{a'_{R^-,1}}{a'_{R^-,2}} = n(pH_1 - pH_2) \qquad (13)$$

or the relative concentrations of the groups, Eq. 14,

$$\frac{\Delta c'_{R^-}}{c'_{R^-,2}} = 10^{n(pH_1 - pH_2)} - 1 \qquad (14)$$

(referred to pH_2), since activities of anionic surface groups can be replaced by concentrations due to their minute changes with pH. For example, the anionic surface group activity changes by less than 0.6% when the hydrogen ion concentration changes by an order of magnitude, $\Delta pH=1$, which justifies the assumption of a constant activity coefficient of the negative surface groups, Eq. 15,

$$\frac{d\varepsilon_m}{d\mathrm{pH}} = \left(\frac{d\varepsilon_m}{d \log c'_{R^-}}\right)\left(\frac{d \log c'_{R^-}}{d\mathrm{pH}}\right) = -(1-n)k = \text{const.} \qquad (15)$$

As a consequence, incidentally, the practical electrode slope $(1-n)k$ is independent of the activity coefficient of the negatively charged surface groups and of pH (and pM), Eq. 15, in agreement with experimental observations. However, the linear potential slope was not derived from first principles here but is the consequence of an assumed approximation of a constant activity coefficient in Eq. 15. This may not be absolutely valid within the transition range where the surface coverage of the glass changes (see Eq. 12). However, the constant slope of glass electrodes at 100% pH and 100% pM selectivity has always been observed experimentally, also within the transition range, and has consequently never been questioned or discussed, although it is one of the most significant properties of glass electrodes.

Independent verification of the dissociation mechanism The discovered mechanism of the functioning of glass electrodes was independently verified [17]. For this reason, several pairs of equal types of glass electrodes were applied within their transition range and at equal pH and

pM values for each pair. One electrode of each pair was subjected to surface analysis by IBSCA yielding relative surface concentrations of RH and RM and thus the ("analytical") selectivity product, Eq. 16a,

$$\left(K_{\mathrm{D,H}}K_{\mathrm{A,M}}\right)_{\mathrm{IBSCA}} = \left(\frac{a'_{\mathrm{RM}}a_{\mathrm{H_3O^+}}}{a'_{\mathrm{RH}}a_{\mathrm{M^+}}}\right)_{\mathrm{IBSCA}}. \tag{16a}$$

The other electrode subjected to potentiometric measurements resulted in the ("potentiometric") selectivity product, Eq. 16b,

$$\left(K_{\mathrm{D,H}}K_{\mathrm{A,M}}\right)_{\mathrm{pot}} = \left(\frac{a'_{\mathrm{RM}}a_{\mathrm{H_3O^+}}}{a'_{\mathrm{RH}}a_{\mathrm{M^+}}}\right)_{\mathrm{pot}}. \tag{16b}$$

For each pair of electrodes, the different selectivity products, Eqs. 16a and 16b, were found to be numerically equal within the limits of error independent of the relative pH and pM and of the membrane glass, which shows that both equilibria, the one determining the surface coverage and the one giving the potential difference of the glass surface, are identical. This result, in turn, exhibits the validity of the dissociation mechanism.

Glass electrodes in heavy water solutions

General It had been known that glass electrodes function as well in heavy water solutions as they do in light water solutions when the investigation of the glass electrode mechanism began at the Schott Electrochemical Laboratory [27]. It is however noted that D_2O is not just another one of the many non-aqueous solvents, but that it is distinguished by the isotopic acidic component, the deuteron (D^+) or deutonium (D_3O^+) ion. Therefore, the application of glass electrodes in this solvent and not in any other non-aqueous solvent was treated at the Electrochemical Laboratory, although the mechanism of its pD response equals strongly that of its pH response [28]. Even a sub-ideal response and its consequences were measured. The response of glass electrodes, including that in heavy water solutions, is thus given quite generally by Eq. 17,

$$\frac{\mathrm{d}\varepsilon_{\mathrm{m}}}{\mathrm{dpX}} = -\left(1 - \frac{\mathrm{d}\left(\log a'_{\mathrm{R^-}}\right)}{\mathrm{dpX}}\right)k = -\alpha_{\mathrm{gl}}k, \tag{17}$$

and the rigorous electrode potential difference by Eq. 18,

$$\varepsilon_{\mathrm{m}} = \varepsilon^0_{\mathrm{X}} - \left[1 - \frac{\mathrm{d}}{\mathrm{dpX}}\left(\log\frac{a'_{\mathrm{R^-}}}{a'_{\mathrm{RX}}a_{\mathrm{H_2O}}}\right)\right]k\mathrm{pX} = -\alpha_{\mathrm{gl}}k\mathrm{pX}, \tag{18}$$

where X is H, D, M(H_2O), or M(D_2O); R^- is any functional glass surface group; and α_{gl} is the electromotive efficiency. pD, similar to pH, is defined by Eq. 19,

$$\mathrm{pD} = -\log\frac{a_{\mathrm{D}}}{m^0}, \tag{19}$$

where m^0=1 mol kg^{-1} [29].

Operational meaning of δ_{glass}: deuteron effect Before the assignment of pD(S) values for the standardization of glass electrode cells, an empirical method for determining pD values had been reported, frequently verified, and thoroughly investigated. The procedure consists of the measurement of the apparent (or operational) $\mathrm{pH^D}$ measured in a solution in heavy water by means of a glass electrode cell calibrated in standard buffers in light water and the addition of an empirical correction term δ_{glass}, Eq. 20,

$$\mathrm{pD} = \mathrm{pH^D} + \delta_{\mathrm{glass}}, \tag{20}$$

whose numerical value has been given as 0.41 on the molar scale and as 0.45 on the molal scale. We call this effect deuteron effect [30].

It was of high interest to understand the meaning of the deuteron effect and to secure that the numerical values given are constant, as claimed, in order to exclude any faulty data from further research. This question was investigated by a glass electrode cell calibrated by multiple-point calibration with linear regression [31] by using standard buffer solutions in light and heavy water. The cell has the respective calibration functions, Eq. 21,

$$E_{\mathrm{H}} = E^0_{\mathrm{H}} - k'_{\mathrm{H}}\mathrm{pH}, \tag{21}$$

and Eq. 22,

$$E_{\mathrm{D}} = E^0_{\mathrm{D}} - k'_{\mathrm{D}}\mathrm{pD}, \tag{22}$$

where E^0_{H} and E^0_{D} are respective standard potential differences, and k' is the average practical slope indicated. Application of the cell in a solution in D_2O yields an emf that represents the emf $E^{\mathrm{D}}_{\mathrm{H}}$ and the related apparent $\mathrm{pH^D}$ on the light water calibration line, Eq. 23,

$$\mathrm{pH^D} = \frac{E^0_{\mathrm{H}} - E^{\mathrm{D}}_{\mathrm{H}}}{k'_{\mathrm{H}}}, \tag{23}$$

and the emf E_{D} and the pD on the heavy water calibration line, Eq. 24,

$$\mathrm{pD} = \frac{E^0_{\mathrm{D}} - E_{\mathrm{D}}}{k'_{\mathrm{D}}}. \tag{24}$$

From Eqs. 23 and 24, the correction factor is obtained by Eq. 25 (see also Fig. 1),

$$\mathrm{pD} - \mathrm{pH^D} = \delta_{\mathrm{glass}} = \frac{E_{\mathrm{D}}^0 - E_{\mathrm{H}}^0}{k'}, \tag{25}$$

because $k_{\mathrm{H}}^{'} = k_{\mathrm{D}}^{'} = k'$ with good approximation and, according to the multiple-point calibration procedure, $E_{\mathrm{D}} = E_{\mathrm{H}}^{\mathrm{D}}$. The liquid junction voltage ε_{j}, which is actually contained in E, does not appear in the operational equation because also $E - \varepsilon_{\mathrm{j}} = E_{\mathrm{D}} = E_{\mathrm{H}}^{\mathrm{D}}$. The correction term δ_{glass} is thus indeed independent of the liquid junction voltage if multiple-point calibration is applied.

Mechanistic meaning of δ_{glass} In addition to the operational equation, the mechanistic meaning of the correction term was derived in order to obtain information on the origin of this number. For this reason, the standard potential differences of cell, Eq. 26, with light and heavy water,

$$\begin{aligned}&\text{ref. el.}|\mathrm{KCl(soln)},\ \mathrm{H_2O}\|\text{soln},\mathrm{H_2O},\mathrm{pH}|\text{glass membrane}\\ &\quad|\text{int.buffer}|\text{int. ref. el.}\end{aligned} \tag{26}$$

were analyzed. Cell (Eq. 26) with light water, for example, consists of all potential differences involved and is represented by Eq. 27,

$$E_{\mathrm{H}} = \varepsilon_{\mathrm{m,H}} + \varepsilon_{\mathrm{j,m,H}} + \varepsilon_{\mathrm{j,H}} + \sum \varepsilon_{\mathrm{n}}, \tag{27}$$

where $\varepsilon_{\mathrm{m,H}}$ is the phase boundary potential difference at the interface membrane/measuring solution, $\varepsilon_{\mathrm{j,H}}$ is the liquid junction voltage between the reference and the measuring solution, $\varepsilon_{\mathrm{j,m,H}}$ is the liquid junction voltage within the leached layer below the external membrane surface, and $\sum \varepsilon_{\mathrm{n}}$ is the sum of all constant potentials of cell (Eq. 26). $\varepsilon_{\mathrm{m,H}}$ is given by the dissociation equilibrium of the protonated (SiOH) surface groups, whose shortest version is represented by Eq. 28,

$$\varepsilon_{\mathrm{m,H}} = -k \log K_{\mathrm{D,H}} - k_{\mathrm{gl,H}}\mathrm{pH}, \tag{28}$$

where $K_{\mathrm{D,H}}$ is the heterogeneous dissociation constant, and $k_{\mathrm{gl,H}} = \alpha_{\mathrm{H}} k$ is the practical glass electrode slope with α_{H}= electromotive efficiency of the glass electrode. Introducing the phase boundary potential (Eq. 28a) into (Eq. 26) yields the emf of cell (Eq. 26),

$$E_{\mathrm{H}} = -k \log K_{\mathrm{D,H}} + \varepsilon_{\mathrm{j,m,H}} + \sum \varepsilon_{\mathrm{n}} - k_{\mathrm{gl,H}}\mathrm{pH} + \varepsilon_{\mathrm{j,H}}, \tag{28a}$$

the first three terms on the right side of which represent the standard potential of the calibration function, Eq. 23, of cell (Eq. 26) with light water,

$$E_{\mathrm{H}}^0 = -k \log K_{\mathrm{D,H}} + \varepsilon_{\mathrm{j,m,H}} + \sum \varepsilon_{\mathrm{n}}, \tag{29}$$

which is required for the mechanistic interpretation of the correction term, Eq. 25.

An analogous derivation yields the emf of cell (Eq. 26) with heavy instead of light water and the standard potential of the calibration function of cell (Eq. 24) with heavy water,

$$E_{\mathrm{D}}^0 = -k \log K_{\mathrm{D,D}} + \varepsilon_{\mathrm{j,m,D}} + \sum \varepsilon_{\mathrm{n}}. \tag{29a}$$

Introducing the standard potentials, Eq. 29 and Eq. 29a, into the operational equation, Eq. 25, finally yields the mechanistic expression of the correction term, Eq. 30,

$$\delta_{\mathrm{glass}} = \log \frac{K_{\mathrm{D,H}}}{K_{\mathrm{D,D}}} + \frac{\Delta\varepsilon_{\mathrm{j,m}}}{k}, \tag{30}$$

because, with good approximation, $k'=k$. The difference of the diffusion potentials in the isotopically leached layers of the membrane glass, $\Delta\varepsilon_{\mathrm{j,m}} = \varepsilon_{\mathrm{j,m,D}} - \varepsilon_{\mathrm{j,m,H}}$, may be called "residual diffusion potential of the isotopically leached layers" in analogy with the residual liquid junction potential between solutions as introduced by Bates (see [1], p. 248f).

Equation 30 shows that contrary to reports in the literature, the correction term is not a universal constant but consists of two individual glass properties, the ratio of the heterogeneous isotopic dissociation constants and the residual diffusion potential of the isotopically leached layers of the membrane glass. This is confirmed by experimental results (Fig. 2), especially by the scatter of data at 25°C and by the different temperature dependence of δ_{glass} for the different surface groups SiO and [SiOAl].

It is to be noted, however, that pH and pD values cannot strictly be compared because they are based on the concept of zero standard potentials of the Pt,H_2 and Pt,D_2 electrodes, respectively. Covington et al. have reported an empirical correction term δ_{gas} for the determination of pD

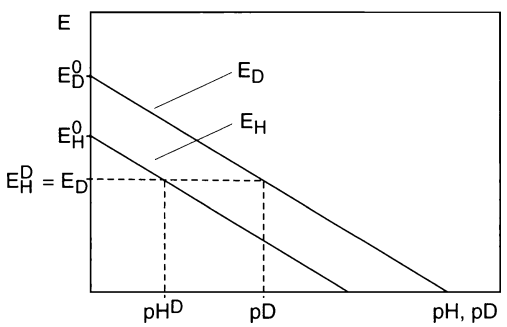

Fig. 1 Sketch of the calibration functions of a glass electrode cell in ordinary and heavy water, demonstrating the operational meaning of the deuteron effect δ_{glass}

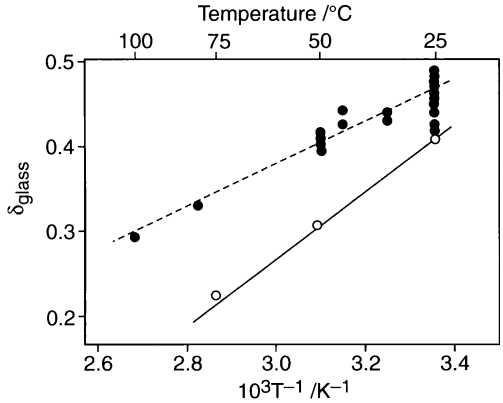

Fig. 2 Correction terms δ_{glass} of pH and pNa glass electrodes from various sources as functions of the reciprocal absolute temperature. *Filled circles*: pH electrodes (SiO surface group), *open circles*: pH funtion of pNa electrodes ([AlOSi] surface group). The data as well as the derivation demonstrate that the correction term is not a universally constant number as generally believed

by means of Pt,gas electrodes, which can be expressed operationally as well as mechanistically by Eq. 31,

$$pD_g - pH_g^D = \delta_{gas} = \frac{E^0_{Pt,D_2} - E^0_{Pt,H_2}}{k'_g} = \frac{\varepsilon^0_{Pt,D_2} - \varepsilon^0_{Pt,H_2}}{k'_g}, \quad (31)$$

where E^0 and ε^0 are standard emf and standard potential, respectively, of the respective cell and Pt,gas electrode indicated. Equation 32 thus yields absolute ratios of the heterogeneous dissociation constants,

$$\log\frac{K_{D,H}}{K_{D,D}} = \left(\delta_{glass} - \frac{\Delta\varepsilon_{j,m}}{k}\right) - \delta_{gas}, \quad (32)$$

by subtracting δ_{gas}=0.072 from Eq. 30. This number was given by Covington [27] and agrees with an experimentally obtained result from Gary et al. [32].

It was found that the average difference of the standard entropies $\Delta\left(\Delta S^0_D\right)_{av}$ of the isotopic dissociation equilibria differs strongly for the pH functions of the different surface groups SiO (pH glass) and [SiOAl] (pNa glass). Obviously, different forms of ions participate in the dissociation equilibria. The SiO^- group seems to combine preferably with protons and deuterons to form SiOH and SiOD, whereas the $[SiOAl]^-$ group probably prefers hydronium and deutonium ions to form $[SiOAl](H_3O)$ and $[SiOAl](D_3O)$ entities [33]. The cause could be the dislocated electron of the $[SiOAl]^-$ arrangement which, unlike the electron located at the oxygen of the SiO^- group, does not favor the dissociation of, respectively, hydronium and deutonium ions into protons and deuterons and water and heavy water molecules. Besides, the spatial conditions of the [SiOAl] site, which is known to favor the association with alkali ions over that with protons and deuterons (see alkali-sensitive glass electrodes) [34], are expected to combine with hydronium and deutonium rather than with protons and deuterons.

An observation by Lowe and Smith is of interest in connection with the treated subject. These authors observed small potential drifts after glass electrodes had been transferred between the isotopic solvents, which depended on the square root of time indicating diffusion control. Indeed, our infrared measurements revealed that the effect was caused by the exchange of the isotopes in the leached layers of the membrane glasses, that is, the authors had measured the "residual diffusion potential" (see above) [35]. Although the effect is small (less than 1.5 mV corresponding to $\delta_{glass} \leq 0.025$), it should be observed when exact pD values are to be obtained by means of glass electrodes on the basis of the deuteron effect.

Deuterium oxide effect

Also, an empirical method for determining $pNa(D_2O)$ values of sodium-containing solutions in heavy water has been given in the literature (see [1], p. 252). It is completely analogous to the method of determining the deuteron effect. The apparent $pNa(H_2O)^{D_2O}$ in the heavy water solution measured by means of a glass electrode cell calibrated in standard sodium solutions in light water is converted into $pNa(D_2O)$ by adding a correction term $\delta_{glass,Na}$, Eq. 33,

$$pNa(D_2O) = pNa(H_2O)^{D_2O} + \delta_{glass,Na}, \quad (33)$$

whose magnitude has been estimated to be 0.09±0.02 on the molar scale that corresponds to 0.13±0.03 on the molal scale. The effect is called deuterium oxide effect.

Operational equation The operational equation as well as the mechanistic meaning of the pNa correction term can be obtained in analogy with those of the pH correction term. The glass electrode is a sodium-selective glass electrode at 100% sodium response calibrated by means of standard sodium solutions in heavy and in light water. When the cell is applied in a sodium-containing solution in heavy water, it yields an emf that characterizes the apparent pNa in light water on the light water line, Eq. 34,

$$pNa(H_2O)^{D_2O} = \frac{E^0_{Na(H_2O)} - E^{D_2O}_{Na(H_2O)}}{k'}, \quad (34)$$

and the $pNa(D_2O)$ in heavy water on the heavy water line, Eq. 35,

$$pNa(D_2O) = \frac{E^0_{Na(D_2O)} - E_{Na(D_2O)}}{k'}, \quad (35)$$

Combining these equations yields the operational expression of the pNa correction term, Eq. 36,

$$\mathrm{pNa(D_2O)} - \mathrm{pNa(H_2O)}^{\mathrm{D_2O}} = \delta_{\mathrm{glass,Na}} = \frac{E^0_{\mathrm{Na(D_2O)}} - E^0_{\mathrm{Na(H_2O)}}}{k'} \quad (36)$$

in a way completely analogous to the derivation of the correction term for heavy water solutions.

Mechanistic meaning of $\delta_{glass,Na}$ The mechanistic meaning of the pNa correction term is also obtained in a way analogous to the meaning of the deuteron effect and results in Eq. 37,

$$\delta_{\mathrm{glass,Na}} = \log \frac{K_{\mathrm{A,Na(D_2O)}}}{K_{\mathrm{A,Na(H_2O)}}}, \quad (37)$$

where the term containing the diffusion potentials has cancelled because the surface coverage with RNa groups at 100% sodium response of the glass is independent of the solvent. When the glass contains ions other than sodium, the situation becomes complicated, and the glass must be stored in pNa solutions, also between measurements, in order to keep the surface from taking up alkali ions other than sodium ions.

Selectivities in light and heavy water The different magnitudes of the pD and pNa correction terms result in different selectivity ranges of glass electrodes in the isotopic solvents (see [1], p. 252f). This results from the comparison of the transition pH in light water, Eq. 38,

$$\mathrm{pH_{tr}} = -\log\left(K_{\mathrm{D,H}} K_{\mathrm{A,Na(H_2O)}} a_{\mathrm{Na^+(H_2O)}}\right), \quad (38)$$

with the transition pD in heavy water, Eq. 39,

$$\mathrm{pD_{tr}} = -\log\left(K_{\mathrm{D,D}} K_{\mathrm{A,Na(D_2O)}} a_{\mathrm{Na^+(D_2O)}}\right), \quad (39)$$

for a given membrane glass. Combining these equations, assuming the same sodium activity in the isotopic solutions, and applying the deuteron and sodium correction terms yield the difference of interest, Eq. 40,

$$\mathrm{pD_{tr}} - \mathrm{pH_{tr}} = \delta_{\mathrm{glass}} - \delta_{\mathrm{glass,Na}} - \frac{\Delta\varepsilon_{\mathrm{j,m}}}{k'}. \quad (40)$$

Since this difference is a positive number, pNa glass electrodes are expected to exhibit a slightly wider sodium-selective range in H_2O than in D_2O (Fig. 3) and pH glass electrodes to exhibit a smaller sodium error in heavy than in ordinary water solutions. From reported correction terms and residual diffusion potentials, it follows that $(\mathrm{pD_{tr}} - \mathrm{pH_{tr}}) = 0.30 \pm 0.08$, which should well be measureable under good experimental conditions.

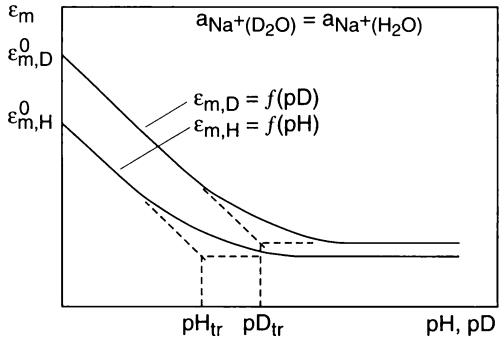

Fig. 3 Schematic of glass electrode response in the transition range between pH and pNa(H_2O) in light water and between pD and pNa (D_2O) in heavy water at an equal sodium activity demonstrating slightly different alkali errors in the two solvents

Hydrogen-sensitive platinum-covered glass electrode membranes

Aim of the measurements The glass electrodes treated in the following brief section had 100% protonated, alkali-free (as shown by IBSCA) external glass surfaces, were covered with platinum layers, and contacted with hydrogen gas-containing atmospheres. The aim of these measurements was to study the interface between protonated glass and hydrogen-contacted platinum at ambient temperatures up to 95°C, that is, at application temperatures of glass electrodes. Measurements on platinized vitreous silica had been reported earlier. However, they were carried out at 1,000°C [36] and between 700°C and 900°C [37], and the different aim was to obtain transport numbers of protons in vitreous silica.

Experimental set-up The electrochemical cell had the cell scheme, Eq. 41,

$$\text{Int. ref. electrode}|\text{int. ref. buffer}|\text{glass, protonated glass}|\mathrm{Pt,H_2}(p_{\mathrm{H_2}}), \quad (41)$$

whose emf is given by Eq. 42,

$$E = \sum \varepsilon_1 + \varepsilon_{\mathrm{gl/Pt}}, \quad (42)$$

where $\sum \varepsilon_1$ is the sum of all internal potential differences of the glass electrode, and $\varepsilon_{\mathrm{gl/Pt}}$ is the potential difference at the protonated glass/platinum interface. Measurements of the emf's of the same cell at two different hydrogen partial pressures thus yield the simple Eq. 43,

$$\Delta E = E_2 - E_1 = \varepsilon_{\mathrm{gl/Pt,2}} - \varepsilon_{\mathrm{gl/Pt,1}}, \quad (43)$$

Experimental results emfs of cell (Eq. 41) as functions of temperature (11 temperatures each) were found to be straight lines between 15°C and 95°C at four different hydrogen partial pressures between 10^{-4} and 1 bar. The measurements were taken in arbitrary order, which caused no changes of the results and obviously no impairment of the Pt layers and the protonated glass, even at the highest temperatures. The measured hydrogen functions ("hydrogen slopes"), $\Delta\varepsilon_{gl/Pt}/\Delta\log p_{H_2}$, differed from the theoretical values $-2.303RT/2F$ by less than ±0.5% at all temperatures, and the temperature dependence of the electrode slopes, $\Delta\left(\Delta\varepsilon_{glass/Pt}/\Delta\log p_{H_2}\right)/\Delta T$ agreed with theoretical values within ±0.2%. The Pt,H_2 electrode in contact with protonated glass thus exhibits the same hydrogen response as does the platinized platinum/hydrogen electrode in aqueous solutions, where it is one of the most reliable electrodes. The critical points of the measurements were (1) the absence of traces of alkali ions, which was shown by IBSCA measurements; (2) the absence of traces of water, which was given by the strong proton acceptor action of siloxy groups; and (3) the absence of potential formation due to arbitrary proton adsorption to the glass surface, which is extremely improbable as long as siloxy groups are present, because the chemical bond of protons to the acceptor groups SiO^- is much stronger than the adsorption bond of protons to any undefined locus of a glass surface.

The only surface reaction that can be imagined is thus the one given by Eq. 44,

$$\frac{1}{2}H_2(Pt)+SiO^-(s)\rightleftarrows SiOH(s)+e^-(Pt), \tag{44}$$

where the bracketed (s) means glass surface. The thermodynamic equation of the reaction is, Eq. 45,

$$\varepsilon_{gl,Pt}=\varepsilon^0_{gl,Pt}+\frac{RT}{F}\ln\frac{a'_{SiOH}}{a'_{SiO^-}}-\frac{RT}{2F}\ln p_{H_2}, \tag{45}$$

and the version including the sub-ideal response is, Eq. 46,

$$\frac{d\varepsilon_{gl,Pt}}{d\log p_{H_2}}=-\frac{k}{2}\left[2\frac{d\log a'_{SiO^-}}{d\log p_{H_2}}+1\right]. \tag{46}$$

Thus, in principle, also the potential of the protonated glass/Pt,H_2 electrode exhibits a sub-ideal response, but the effect is too small to be measured due to the larger uncertainties of the measurements involving the solid materials. The approximate slope is thus, Eq. 47,

$$\frac{d\varepsilon_{gl,Pt}}{d\log p_{H_2}}=-\frac{k}{2}=-\frac{2.303RT}{2F}, \tag{47}$$

and the temperature dependence of the slope is, Eq. 48,

$$\frac{d}{dT}\left(\frac{d\varepsilon_{gl,Pt}}{d\log p_{H_2}}\right)=-\frac{k}{2T}=-\frac{2.303R}{2F} \tag{48}$$

$$=-9.92\times10^{-2}\,\mathrm{mV\,K^{-1}\,at\,25\,^{\circ}C}.$$

The significant result of these measurements is that the membrane glass participates in the formation of the phase boundary potentials with its functional surface groups independent of whether the contacting phase is an electrolyte solution, as in the case of glass electrodes,

$$SiOH(s)+H_2O(soln)\rightleftarrows SiO^-(s)+H_3O^+(soln), \tag{49}$$

or a solid, as with a Pt,H_2 electrode,

$$SiOH(s)+e^-(Pt)\rightleftarrows SiO^-(s)+\frac{1}{2}H_2(Pt). \tag{50}$$

In both cases, the proton acceptor is the siloxy group at the glass surface. The proton donor of the contacting phase is the hydronium ion of the solution and the catalytically dissociating hydrogen molecule of the Pt,H_2 electrode. Both reactions cause a phase separation and an equal galvanic potential difference, independent of the material that contacts the membrane glass.

Phosphate and fluoride error of pH glass electrodes

The phenomenon We detected the phosphate error when pH glass electrodes were kept in a phosphate-containing buffer solution for an extended length of time. Although all conditions remained unchanged, the primarily constant potential started to change to more negative values without any visible reason after about 1 h at 50°C (Fig. 4). The change was approximately linear and lasted over 2 h, i.e.,

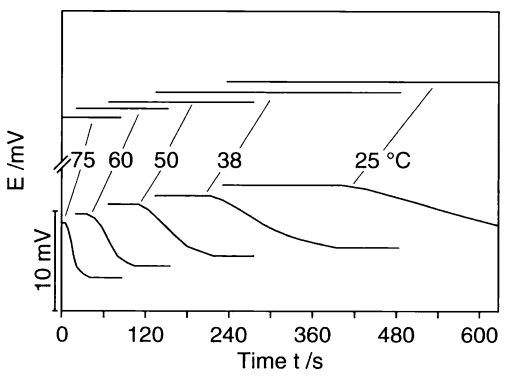

Fig. 4 Temperature dependence of phosphate error of a pH glass electrode with lanthanum-containing membrane as compared to a glass electrode with lanthanum-free membrane (upper constant potentials)

for −5 mV, after which time, it attained a constant value again. When the electrode was subsequently transferred into a phosphate-free solution with lower pH, its potential changed back to more positive values and returned to its initial potential in about 3 h, however, not stepwise but in an asymptotic way. The effect was shown to be strongly temperature-dependent (Fig. 5).

The cause of the effect Further studies yielded that the effect appeared if the membrane glass of the electrode contained lanthanum. This element has been recommended by Perley as small addition to the glass because it improved melting and glass blowing conditions [38, 39]. However, no designer of electrode glasses ever took into account that lanthanum orthophosphate (and lanthanum fluoride) have extremely low solubilities. The extremely small solubility product even comes into play when lanthanum-containing glasses are in contact with phosphate (or fluoride)-containing solutions [40] as, for example, phosphate buffers. The reactions are of particular interest because the formation of various stages of the minute precipitates can be followed by the characteristic changes of the electrode potential despite the extremely small quantities of the material generated. To give an impression, the solubility product of $LaPO_4$ is $K_{s0} = 10^{-22.4}$ mol dm^{-3} at 25°C [41], which means that a saturated $LaPO_4$ solution contains $10^{-11.2}$ mol dm^{-3} of the salt if the solution is otherwise free of phosphate, and as little as $10^{-21.4}$ mol dm^{-3} of lanthanum ions if, for instance, the total phosphate concentration is 0.1 mol dm^{-3}. The condition for these numbers is pH≥13. This, in addition, shows the complicated conditions: The solubility of $LaPO_4$ depends strongly on the solution pH because the orthophosphate ion concentration determining the concentration of lanthanum ions is itself a strong function of pH [42]. For instance, at a given total phosphate concentration, the concentration of lanthanum ions increases by nearly six orders of magnitude when the pH is decreased from pH=7 to pH=4. The physicochemical basis of these solubility phenomena is thoroughly discussed in [43, 44].

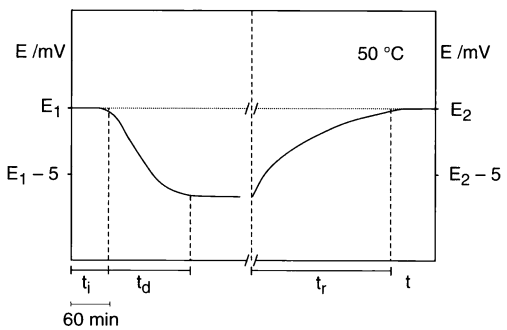

Fig. 5 Phosphate error of a pH glass electrode with lanthanum-containing membrane. t_i = induction time, t_d = drift time, t_r = recovery or return time

Investigation of the phosphate error The "error" was investigated, inter alia, by means of scanning electron microscope, energy dispersive X-ray, and IBSCA with the following result. The lanthanum, being a network former [45], is slowly released into the solution with the constant rate of the glass dissolution if the leached layer of the silicate membrane glass is in a steady state. As soon as the lanthanum ions come into contact with phosphate ions (if the solution contains phosphate), it forms lanthanum orthophosphate, which precipitates on the glass surface, probably as non-crystalline patches or groups. As long as the precipitate does not form a phase able to generate an independent potential, the potential of the glass is solely controlled by the pH of the solution as expected. During this period, the potential is constant and is called *induction time* t_i. However, when the amount of the precipitated lanthanum phosphate suffices to form crystals, the larger crystalline patches act as a phase in contact with the glass and the solution and form a mixed potential that is thermodynamically given by the lanthanum content of the glass and the saturated solution directly at the glass surface. The potential changes due to the following increase of the surface coverage with crystalline lanthanum phosphate, and this time is called the *drift period* t_d. Finally, the potential attains a constant value when the glass surface is completely covered with a monolayer of the crystalline salt, which probably consists of unit cells, at the end of t_d. Because hexagonal $LaPO_4$ has a rather open structure and is transparent to water molecules and thus to hydronium ions, the salt layer does not isolate the glass surface from the solution but allows the existence of the potential of the glass in addition to its own potential so that the membrane exhibits a constant mixed potential, which is the "faulty" potential observed after the drift period. Further precipitation of $LaPO_4$ can only increase the thickness of the salt layer but does not influence the membrane potential. Unlike the formation, the dissolution of the salt layer at lower pH (and thus higher solubility) does not show any characteristic steps and thus proceeds asymptotically during the restoring time t_r as observed by the continuous increase of the potential. The given mechanism was quantitatively concluded from the results of the surface measurements given above.

Possible consequences of the phosphate error In general, glass electrodes contain an internal buffer solution, which cannot be exchanged. If the membrane glass contains lanthanum and the internal solution is a phosphate buffer, the electrode exhibits a "reverse or internal phosphate error," i.e., the potential of the electrode shows a positive deviation from the normally expected value and exhibits a possibly inconstant irreversible "asymmetry potential." This effect can easily be accounted for by omitting internal

phosphate buffers if the cause is known. This, however, has not been the case before we detected the phosphate error, and glass electrodes produced in order to test newly developed membrane glasses may often have shown such "unsatisfying potentials," and the membrane glasses tested may have been discarded, although they were excellent glasses — forming constant potentials in the absence of phosphate and/or if they contained no lanthanum. However, nobody can even guess the damage that was indirectly caused by the phosphate error.

Electromigration of cations in glasses

Application of IBSCA: the analytical basis The introduction of IBSCA into the work of Schott Electrochemical Laboratory meant completely new fields of research because this technique revealed information on ion concentrations and movements in glass regions of unforeseen small dimensions. In addition to elucidate the mechanism of glass electrodes as described above, it was thus of high interest to investigate the response of cations and related changes of their surroundings to electric fields, that is, to investigate the electrolysis of solid glasses (see [1], pp. 96–151). The materials of immediate interest were the lithium ion-conducting glasses, lithium silicate and lithium alumosilicate, and lithium ions and protons since it could be expected that both ions could be introduced (lithiation and protonation) and replaced by each other in these materials. The most interesting case to be investigated was certainly the simultaneous introduction of both ions which, however, required information about the one-ion electromigration, because this would give a necessary basis and would exclude misinterpretations because of erroneous assumptions when two ions were to be investigated.

Electromigration of guest protons and of guest deuterons The first and basic experiments were the protonation and deuteration of a lithium silicate and a lithium alumosilicate glass and the subsequent measurement of the resulting concentration profiles by means of IBSCA. The respective concentration profiles of the elements in either glass were rather similar. However, it became soon obvious that glass samples subjected to quantitative migration experiments had to be brought into an identical thermal (standard) state because the rate-determining average mobilities of lithium ions can differ by a factor of up to six.

It was also found that protons and deuterons, and not the respective hydronium and deutonium ions, enter lithium-containing glasses. This was verified by applying three different anodic materials, protonic non-aqueous solutions, onto the glass precipitated platinum layers in dry hydrogen, and by applying NRA analyses, all of which yielded identical concentration profiles which, in addition, were also identical with profiles obtained from electrolyses with aqueous anodic solutions.

Internal and external stress in protonated glasses The replacement of lithium ions by protons (deuterons) generates void space in the glass network so that protonated and partly protonated layers are subject to some internal and also external tensile stress, which is exerted by the underlying membrane. Both effects influence the ion mobility in the layers, although probably by a small degree, that must be distinguished from each other. Internal stress is an intrinsic property of protonated glasses, which cannot be released by cooling because of the condensation of OH groups at the high temperatures before the cooling process. Ionic mobilities of protonated glasses are thus properties of glasses which are necessarily under internal tensile stress even if the layers are separated from the underlying membrane. However, all experiments conducted showed that the effect of internal stress of protonated and partly protonated layers are rather small if not negligible. External stress could be eliminated by separating the layer from the underlying glass if this were feasible, but also its effect on the mobilities seems insignificant because, according to our measurements, concentration-dependent mobilities of lithium ions and protons in partly protonated glasses, which were determined on layers with rather different thicknesses, agreed within the limits of experimental error. Vice versa, the compressive stress exerted by the thin protonated layer on the underlying much thicker membrane certainly decays with depth within short distances and is not expected to affect the mobility of the lithium ions of the unchanged glass either.

Transfer of different cations across the interface solution/glass: the experimental phenomenon The simultaneous transfer of two different ion species from an anodic solution into glass was studied with lithium ions and protons because it was (quite correctly) expected that these ions could be introduced into glasses without any steric difficulties. The glasses chosen were a lithium alumosilicate pNa glass and a lithium silicate pH glass. It was, however, highly surprising that the initially applied anodic solution of lithium and hydronium ions at an arbitrarily chosen concentration ratio of about 10 (pH-pLi=1) caused a lithium mole fraction of only x_{Li}=0.08 in the pNa glass and even x_{Li}=0 in the pH glass. As expected, the lithium mole fraction transferred into the pNa glass increased when the relative activity of the lithium ions in the anodic solution was increased and became 100% at pH-pLi=4. Even more surprising, however, was that the pH glass was still 100% protonated by the application of this solution,

started to take up lithium ions at pH-pLi=9, and was finally 100% lithiated at (pH-pLi)≥12.5. Indeed, a protonated layer with equal mole fractions of the ions, $x_H=x_{Li}=0.5$, in the pH glass necessitated an anodic solution with a lithium activity that was $10^{10.5}$ times that of the hydronium ions!

The extreme ionic ratios observed, especially that exhibited by the pH glass, suggested strongly that the glass surface does not act as an inert plane that is crossed by the ions simply according to their competing activities in the solution, but that a mechanism must be at work that is based on glass properties. The numbers measured even suggested that the transfer was controlled by the interfacial equilibrium between glass surface groups and ions in the solution that determined also the selectivity of glass electrodes, and indeed, this idea could be verified by quantitative measurements.

The quantitative control of ion transfer The equation of the equilibrium between glass surface and cations in the solution was obtained from the sum of the equilibria Eqs. 1a and 1b, yielding Eq. 51,

$$RH(s) + Li^+(soln) + H_2O(soln) \rightleftarrows RLi(s) + H_3O^+(soln), \quad (51)$$

which is quantitatively described by the selectivity product, Eq. 52,

$$K''_{D,H}K'_{A,Li} = \frac{c'_{RLi}a_{H_3O^+}}{c'_{RH}a_{Li^+}}, \quad (52)$$

if the activity of water is taken to be unity. Expressing surface concentrations by mole fractions, $x'_i = \frac{c'_i}{\sum c'_i} = \frac{c'_i}{c'_{i0}}$, yields Eq. 53,

$$x'_{RLi} = 1 - x'_{RH} = \left[\frac{1}{K'_{D,H}K'_{A,Li}}\left(\frac{a_{H_3O^+}}{a_{Li^+}}\right) + 1\right]^{-1}, \quad (53)$$

which is nothing else than Eq. 12 expressed for lithium and hydrogen ions to be transferred into the glass. Figure 6 depicts this equation for a rate-cooled lithium silicate pH glass membrane (solid lines) for three temperatures (25°C, 50°C, and 75°C). The horizontal positions of the lines were adjusted by potentiometrically measured selectivity products. The left ordinate presents calculated equilibrium mole fractions of SiOLi surface groups, and the right ordinate gives lithium mole fractions below the anodic glass surface as measured by IBSCA after electrolyses with appropriate solutions. Figure 7 summarizes the function for a quenched and a rate-cooled lithiumsilicate pH glass and a rate-cooled lithium aluminosilicate pNa glass.

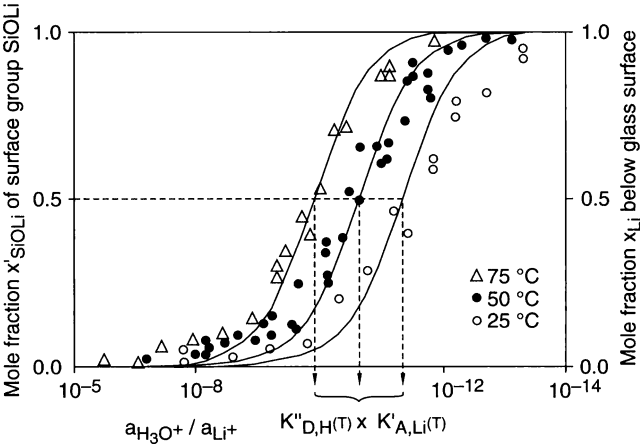

Fig. 6 Dependence of surface state (*left ordinate*) and of ion transfer of a rate-cooled lithium silicate pH glass membrane on the solution composition at various temperatures. *Solid lines* and *left ordinate*: calculated equilibrium mole fractions of SiOLi surface groups whose horizontal positions were adjusted by potentiometrically measured selectivity products. *Dots* and *right ordinate*: lithium mole fractions below anodic glass surface as measured by IBSCA after electrolyses with appropriate anodic solutions

Mechanism of ion transfer through the interface The described experimental observations can be understood by the following transfer mechanism. Cations, e.g., lithium ions and protons, attached to the surface groups and at a dynamic equilibrium with the solution represent the outermost particles of the glass and thus belong to the glass to a much greater extent than to the solution, which means that an electric field across a membrane will extend up to the surface groups. The cations attached to the surface groups will thus follow the driving force of the electric field, and their first successful jump from the surface position into the next available site will be mainly a jump within the glass phase. The relative jump frequency of two different ions leaving the surface groups and thus their relative mobilities through the glass surface, i.e., their mole fraction-dependent average "transfer mobilities" $\overline{u}'(x')$, will be nearly equal to the relative mobilities $\overline{u}(x)$ within the bulk glass, and their transport numbers through the interface or their "transfer numbers," Eq. 53,

$$n'_H = 1 - n'_{Li} = \frac{x'_H\overline{u}'_H(x'_H)}{x'_H\overline{u}'_H(x'_H) + x'_{Li}\overline{u}'_{Li}(x'_{Li})}, \quad (54)$$

will be nearly equal to the mole fraction-dependent transport numbers in the glass,

$$n_H = 1 - n_H = \frac{x_H\overline{u}_H(x_H)}{x_H\overline{u}_H(x_H) + x_{Li}\overline{u}_{Li}(x_{Li})}, \quad (55)$$

where x' and x are mole fractions at the surface and in the glass, respectively.

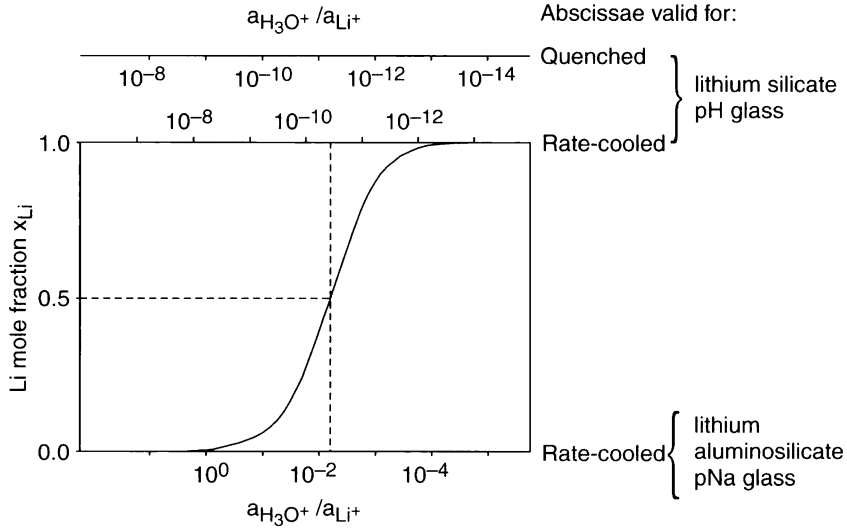

Fig. 7 Comparison of transfer properties of a lithium aluminosilicate pNa glass and of a lithium silicate pH glass at two different thermal histories

Migration of cations after their transfer into the glass Thus, during an electrolysis of a glass membrane, a partly protonated glass layer is generated, the thickness of which increases according to the slow migration of the protons. Simultaneously, lithium ions are also transferred, migrate through this layer according to their larger mobilities, and slow down when they leave the protonated layer so that the relative mole fraction ratio of lithium ions and protons perpendicular to the migration direction, which is given by the transfer number, satisfies the continuity condition. The concentration profile of the protons (and thus also of the lithium ions) and the total charge applied during an electrolysis suffice for the determination of the relative (and absolute) mobilities of the ions.

The supply of cations from the anodic solution to the anodic surface On leaving the surface groups for the glass, the ions are replaced by appropriate ions from the solution so that the surface equilibrium is maintained. This, however, is the case only if the current density i_{el} imposed by the electrolysis is sufficiently smaller than either of the exchange current densities, $i_{0,H}$ and $i_{0,Li}$, of the ions taking part in the equilibrium, because only then is the polarization $\eta = |\varepsilon - \varepsilon_0|$ of the equilibrium, i.e., the shift of the potential ε relative to the equilibrium potential ε_0, small enough to be negligible. Incidentally, a sufficiently small polarization can always be attained by choosing an appropriate current density i_{el} of the electrolysis, Eq. 56,

$$\eta = \frac{RTi_{el}}{Fi_0}. \tag{56}$$

For instance, an electrolysis with a total voltage of 3,500 V on a 0.05-cm thick membrane (field strength, 70 kV cm^{-1}) with a cross-section 1 cm^2 of a glass with a specific resistance $10^{10}\Omega$cm at 25°C causes a polarization of η=1.8 mV if an exchange current density of 10^{-4} Acm^{-2} is assumed. This amounts to a ratio of the electrolysis current density to the exchange current densities of 14.3. The example demonstrates also that the common objection that the application of "high" field strengths to glass membranes changes significantly "the conditions at and below their surfaces" is not justified, but that the critical quantity of glass electrolyses to be kept small is the polarization η of the interfacial equilibrium and not the electric field strength applied across the glass membrane.

Proposal of a simple electromigration mechanism in glasses Electromigration of ions (here lithium ions and protons) can be understood by the following (*perhaps too*) simple mechanism, for which only three assumptions are made:

1. The negative sites are uniformly distributed throughout the glass network.
2. There is no formation of ion clusters.
3. The negative sites are equally available sterically to both lithium ions and protons.

The field-driven migration of an ion, i.e., the probability of an ion to leave its site for a neighboring site, will then depend on

1. The strength of its own bond to the site it occupies,
2. The site concentration, i.e., the average distance between the sites, and
3. The bond strength of the surrounding ions to the sites they occupy.

For a given site concentration, consequently, the following two extreme situations may be visualized:

(A) A cation strongly bound to the site, e.g., SiO^-, it occupies and surrounded mainly by the other ions with a much weaker bond to their sites will preferably leave

its position according to its own bond to the site. This situation is given by a guest proton surrounded mainly by lithium ions, i.e., at low proton concentrations. This is seen by the low mobility ratio of protons to lithium ions at low proton contents, $\overline{u}_{\mathrm{H}}(x_{\mathrm{H}} \to 0)/\overline{u}_{\mathrm{Li}}(x_{\mathrm{Li}} \to 1)$, which is smaller than 6×10^{-3}.

(B) In contrast, the jump probability of a cation only weakly bound to its site but surrounded mainly by ions with a much stronger bond to their sites will be determined by the bond of the surrounding ions to their sites. This situation is approached by a lithium ion surrounded mostly by protons, i.e., by a lithium ion in a highly protonated glass, $\overline{u}_{\mathrm{Li}}(x_{\mathrm{Li}} \to 0)/\overline{u}_{\mathrm{H}}(x_{\mathrm{H}} \to 1)$.

This mechanism can also explain the concentration dependence of the transport data. An exchange of protons for lithium ions in a highly protonated glass is expected to have little effect on the mobilities of both lithium ions and protons. The mobility of lithium ions will not change significantly as long as they are surrounded by immobilizing protons, and the proton mobility remains basically unchanged because of the strong bond to the sites they occupy. On the other hand, replacement of lithium ions at high lithium mole fractions by protons means reducing the concentration of the unhindered, more mobile lithium ions of the glass. It is generally accompanied by a relatively large conductivity decrease, whereas this change will not much influence the mobility of the protons because of their strong bond to the sites. This mechanism is in agreement with experiments, the only exception being the strongly decreasing proton mobility at proton mole fractions below about 0.15, where the structural effect of proton traps becomes detectable, the more so the smaller the proton mole fraction is.

Some properties of glass-forming melts

Thermoelectric voltages In practical glass melting, one has often, if not always, to deal with non-isothermal glass melts, be it because large melt containers, e.g., crucibles, cannot be handled isothermally, or be it because melts in continuous melting tanks are deliberately kept at locally different temperatures because the state of certain reactions, for instance of redox equilibria [46], requires various temperatures and thus temperature gradients. However, temperature gradients cause a "homogeneous polarization" of glass melts due to the preferred direction of polar entities, for example, dipoles and ion couples, along the temperature gradients, and this directional ordering has two consequences:

First, the local atomic electric fields add up along the temperature gradient and cause an electric potential difference between any two points with different temperatures, a phenomenon that is called *Seebeck effect*.

Second, the temperature gradient, in turn, causes thermodiffusion of ions, which is counter-balanced by backdiffusion of the ions due to the generated concentration gradients after some time. This effect is termed *Soret effect*. The buildup time of the steady state of diffusion and counterdiffusion is extremely long in most cases [47], e.g., more than 80 days have been reported for lead-tin melts at 360°C and 600°C. The Soret effect is thus of no concern for glass melting, particularly because industrial glass melts are continuously in motion so that a steady state cannot form.

Seebeck effect The Seebeck effect, however, is of great importance because it often causes serious damages to short-circuited metals submitted to temperature gradients. Measurements of thermoelectric potentials had been performed when we started this work. However, they had been carried out with platinum electrodes, which yielded the sum of thermoelectric and redox potentials of the melts [48, 49]. We realized the measuring errors caused by this shortcoming and the possible consequences for exact results of further measurements. A possible way (and perhaps the only one) was to change the technique by applying so-called "zirconia electrodes" [50], i.e., ZrO_2 tubes with internal platinum (wires) in a gas with defined oxygen partial pressure, for instance with 1 bar, instead of platinum electrodes. Incidentally, zirconia electrodes are usually applied as reference electrodes together with platinum-measuring electrodes for the measurement of the oxygen partial pressure of melts. This application demonstrates the usefulness of our intention and demonstrates that the thermoelectric potentials obtained with zirconia electrodes are free of redox potentials of the melts.

The scheme of the envisaged cell is given by Eq. 57,

$$\mathrm{Pt}'(T_{\mathrm{i}})..\mathrm{Pt}',\mathrm{O}_{2,\mathrm{r}}(T_1) \times \left|\mathrm{ZrO}_2(T_1)\right|\mathrm{melt}(T(\mathrm{x}))\left|\mathrm{ZrO}_2(T_2)\right|\mathrm{Pt},\mathrm{O}_{2,\mathrm{r}}(T_2)..\mathrm{Pt}(T_{\mathrm{i}}), \tag{57}$$

where T_{i} is the temperature of the measuring instruments, T_1 and T_2 are the temperatures of the zirconia electrodes, and T(x) is the locally varying temperature of the melt. It is contained in a 12-cm-long ceramic, e.g., zirconium silicate, boat. The temperature of the non-isothermal melt is supplied by a specially designed temperature furnace. Temperature profiles were directly plotted by pulling a thermocouple connected to a recorder through the melt.

Because of the final extension of the 6-mm-thin zirconia electrodes, the regions of the melt around the sensors were kept isothermal, and the interesting parts of the melt used for the measurements were obtained from the measured temperature profiles.

The thermoelectric emf of cell (Eq. 57) is given by Eq. 58,

$$E_{\Delta T,ZrO_2} = \frac{RT_2}{4F}\ln p_{O_2,r}(T_2) - \frac{RT_1}{4F}\ln p_{O_2,r}(T_1) + E_{Th,m}(T_1,T_2), \quad (58)$$

if the unknown and unattainable quantities are combined as standard thermoelectric emf, Eq. 59,

$$E_{Th,m}(T_1,T_2) = \varepsilon^0_{ZrO_2}(T_2) - \varepsilon^0_{ZrO_2}(T_1) + \frac{RT_1}{2F} \times \ln a_{O^{2-},m}(T_1) - \frac{RT_2}{2F} \times \ln a_{O^{2-},m}(T_2) + \varepsilon_m(T_1,T_2) + \varepsilon_{Pt}(T_2,T_1) \quad (59)$$

Under standard condition of 1 bar oxygen partial pressure around the platinum wires in the zirconia electrodes, the thermoelectric emf is equal to the standard thermoelectric emf, both between the same temperatures, Eq. 60,

$$E_{\Delta T,ZrO_2} = E_{Th,m}(T_1,T_2). \quad (60)$$

The standard thermoelectric emf between two temperatures is given by melt properties, which are principally unknown. However, we could make it probable, at least for certain melts, that it is mainly given by the thermoelectric diffusion potential. Since it is neither necessarily a linear function of the temperature nor of the temperature difference, we have found it useful to define and, in practice, to measure its derivative with respect to the temperature. We thus defined the temperature-dependent *standard Seebeck coefficient*, which is a specific quantity of glass melts and independent of the oxygen partial pressure, Eq. 61a,

$$dE_{Th,m}(T_1,T_2)/d(\Delta T), \quad (61a)$$

or, Eq. 61b,

$$dE_{Th,m}(T_1(T_2 = \text{const}))/dT_1. \quad (61b)$$

It yields the standard thermoelectric emf by integration either for the case of two variable temperatures, Eq. 62a,

$$E_{Th,m}(T_1,T_2) = \int_{T_1}^{T_2} \frac{dE_{Th,m}}{d(\Delta T)}dT, \quad (62a)$$

or for one variable temperature, Eq. 62b,

$$E_{Th,m}(T_1,(T_2 = \text{const})) = -\int_{T_2=\text{const}}^{T_1} \frac{dE_{Th,m}}{dT_1}dT, \quad (62b)$$

where, for example, T_2 is kept constant.

Experimental results The measurements yielded several different types of temperature-dependent standard Seebeck coefficients. To give some examples, Fiolax klar and several other silicate glass melts show a linear temperature-independent standard Seebeck coefficient in the order of −0.4 to −0.6 mV K^{-1}, whereas BK7 exhibits a not quite linear standard Seebeck coefficient of its melt that increases slightly with increasing temperature, i.e., from −0.5 mV K^{-1} at 950°C to −0.3 mV K^{-1} at 1,550°C, and the melt of a phosphate-based optical glass has a standard Seebeck coefficient that decreases non-linearly and more strongly from −0.3 mV K^{-1} at 850°C to −0.95 mV K^{-1} at 1,450°C. The most unexpected result was for a green glass melt, which showed two temperature regions with constant standard Seebeck coefficients, −0.575 mV K^{-1} below and −0.453 mV K^{-1} above 1,020°C. All of these numbers, however, agree in that standard Seebeck coefficients of glass melts are generally negative numbers between −0.1 and −1 mV K^{-1}.

According to cell (Eq. 57), the thermoelectric emf is the result of two influences, a temperature difference and a difference of the oxygen partial pressures in the zirconia electrodes. Rearrangement of Eq. 58 thus allows to compare the relative magnitudes of these different causes, which result in the same effect and compensate each other, Eq. 63,

$$pO_{2,r}(T_1) = \exp\left[\frac{4FE_{Th,m}(T_1,T_2)}{RT_1} + \frac{T_2}{T_1}\ln pO_{2,r}(T_2)\right], \quad (63)$$

The result is in Fig. 8, which shows the log of the ratio of the oxygen partial pressures as a function of the temperature difference of the zirconia electrodes. The

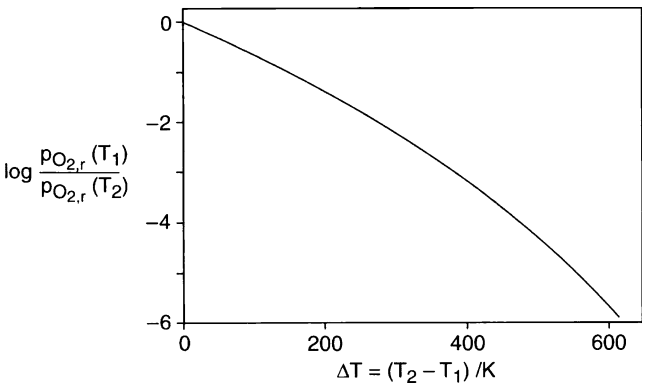

Fig. 8 Compensation of the thermoelectric emf of a cell consisting of two zirconia electrodes at temperatures T_1 and T_2 in a non-isothermal melt by the respective oxygen partial pressures $p_{O_2,r}(T_1)$ and $p_{O_2,r}(T_2)$of the electrodes. Calculations are based on the higher temperature T_2=1,673 K, the oxygen partial pressure of the hot electrode $p_{O_2,r}(T_2 = 1,673\,K) = 1$ bar, and an assumed constant standard Seebeck coefficient $dE_{Th,m}/dT = -0.5\,mV\,K^{-1}$

calculation was based on the higher temperature T_2= 1,673 K, at which the oxygen partial pressure was assumed 1 bar. The standard Seebeck coefficient was assumed constant, and its numerical value is −0.5 mV K^{-1}. The result is surprising indeed: A thermoelectric emf caused by only 150°C (between 1,523 and 1,673 K), for instance, is compensated by a ratio of the oxygen partial pressures in the zirconia electrodes of ten, and this tendency increases with the temperature difference since the curve is not linear.

The conductivity of glass-forming melts

General For economical and ecological reasons, technical glass melting furnaces are increasingly often heated by electricity. Besides, this kind of applying energy to glass melts allows much better process control than heating by flames and thus improves the physical and chemical quality and the homogeneity of the melts and glass products. The Joule effect is applied, i.e., the glass melt is used as the heat resistor, and various metals, e.g., platinum, platinum alloys, and molybdenum, are applied to transfer the necessary energy into the melting units. Because of the difference between electrode and melt volume, the current density and thus the melt temperature increase strongly near the electrode surfaces; glass melts are highly inhomogeneously heated. For producing a glass at a particular temperature, it is thus mandatory not only to know the exact temperature but also the exact temperature dependence of the conductance. When the significance of these relationships were realized at Schott A.G. in the early 1970s, the Electrochemical Laboratory was asked to arrange for exact measurements of temperature-dependent conductances, which meant to set up an appropriate conductance cell. Since, however, the literature did not describe a cell construction that satisfied all required properties, we decided to follow an idea that had developed from the analysis of the reported cells and avoided most of their drawbacks. The cell is meanwhile also applied by several different laboratories [51–55].

Conductance cell designed at Schott A.G. The conductance cell designed at Schott A.G. can best be characterized as immersion-type cell yielding absolute conductances (Fig. 9). The melt is contained in a Pt/10Rh crucible, and the actual cell volume is a volume within the melt that is confined by a vertical alumina (or silica) cell tube introduced into the center of the melt and an upper and a lower platinum electrode. The lower electrode is formed by the upper flat surface of a short cylinder protruding from the crucible bottom into the melt and snuggly surrounded by the lower end of the alumina cell tube. The electrical connection is through the platinum crucible. The lead to the upper platinum electrode is surrounded by a four-bore alumina tube, which carries also the connecting leads to a thermocouple that is situated directly above the upper electrode. The upper electrode is a horizontal cross-shaped design, which can be rotated in order to shear off bubbles that have accidentally been captured and stick to the horizontal lower surface of the metal. The slight non-uniformity of the electric field caused by the cross-shaped electrode is corrected for by a cell length- and conductivity-dependent correction factor determined by means of a plate-shaped electrode. The platinum crucible rests on an alumina piston, from which it is insulated by four alumina support bars, and the entire arrangement is contained in a platinum tube resistance furnace (Pt/20Rh), in which it can be moved vertically for setting up and removing the cell.

Cell characteristics The characteristic properties of the Schott conductance cell are summarized as follows:

The cell yields absolute conductances because the cell constant is determined from the geometrical cell dimensions at each measuring temperature, $C(T_m) = l(T_m)/A(T_m)$, thus avoiding the application of standard melts.

Due to the location of the actual cell volume within the bulk of the melt, measuring temperature, cell constant, and melt density are uniform within the entire cell tube, and the cell constant is independent of the surface tension of the melt.

Evaporation of melt components is excluded because of the position of the actual cell volume below the melt surface.

Stray currents through the hot atmosphere are eliminated by the insulating alumina tubes, which surround all connecting leads.

Disturbing bubbles are removed by rotating the described cross-shaped upper electrode.

The defined variations of the cell length during measurements allow a repetition of measurements and thus the detection of fortuitous impairments of the cell as, for example, a slight dissolution or insufficient resistivity of the cell tube.

The overall reproducibility was determined to amount to $\Delta\sigma = \pm 0.015\sigma$, and the overall uncertainty to approximately 4% of the conductance measured. It includes the temperature uncertainty, which is the highest uncertainty, but which is not specific to the conductance cell.

Mixed alkali glass melts as measured by the Schott conductance cell The mixed alkali effect is usually known as a property of solid glasses (e.g., [56, 57]). Only few papers on this effect of conductance in the molten state have been published, and those which did appear were restricted to temperatures below 1,400°C, relatively large temperature intervals, and only three mole fraction ratios of each alkali couple besides the single alkalis [58–60]. The

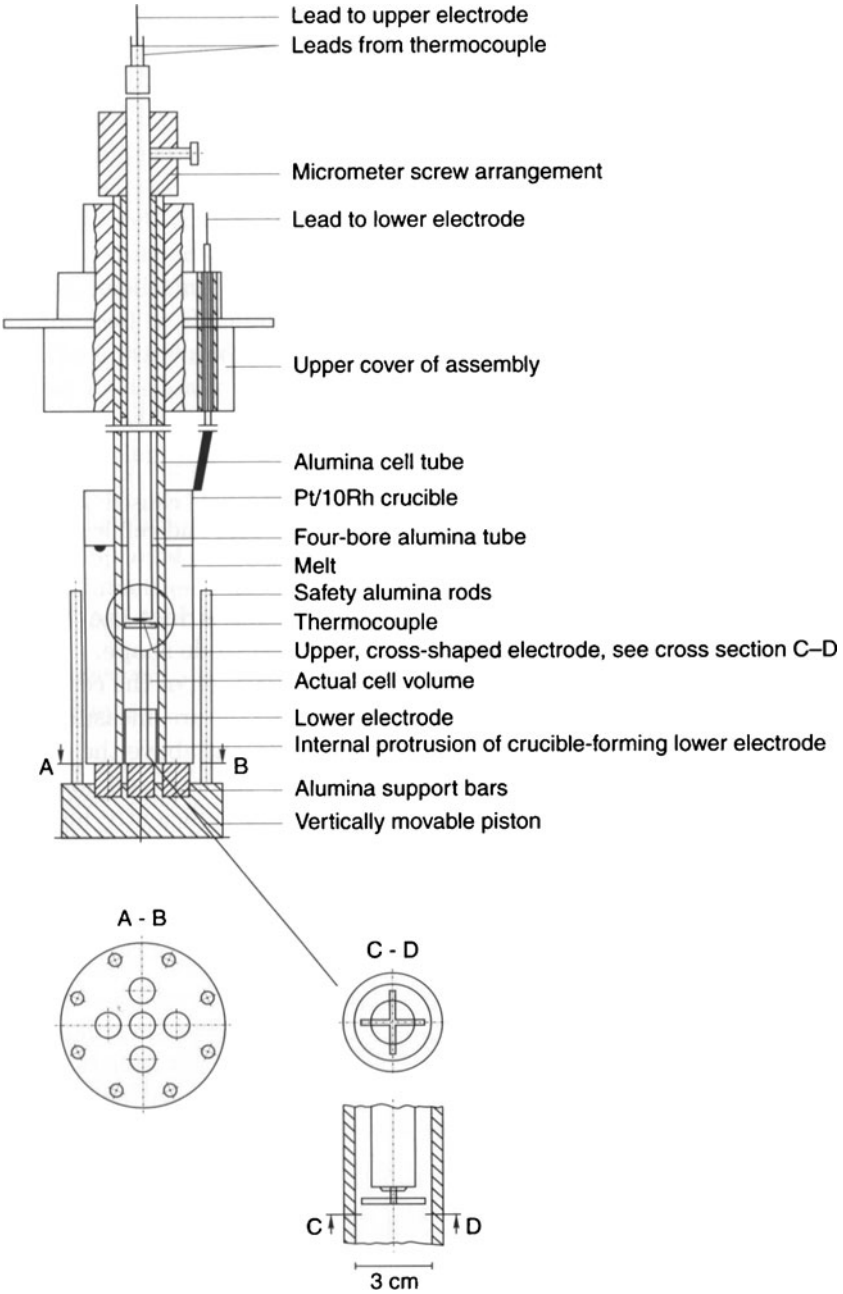

Fig. 9 Vertical cross-section of the conductance cell for glass and salt melts developed by Schott Glas (see text)

analysis of the Schott conductance cell (see above) thus encouraged us to apply the cell also to the more critical measurements of a mixed alkali glass. The glass system $(1-x)Na_2O \cdot xK_2O \cdot 0.7CaO \cdot 4.8SiO_2$ was applied. It consisted of nine glasses with different mole fractions x of the alkalis (x=0, 0.125, 0.250, 0.375,…1.0). Besides, the glasses contained 0.04% Sb_2O_3 as a fining agent. Conductivity measurements were carried out at 50°C temperature intervals between 900°C and 1,550°C and evaluated by the computer program ASYST (Hewlett Packard, Palo Alto, CA, USA). Because of the consistency of the results, we dared to extrapolate the data from 1,550°C to 2,000°C.

Figure 10a, b shows the results for the conductance and activation energy of conductance. Both sets of data exhibit extrema, which are positioned at a potassium mole fraction x=0.7±0.02. However, the minimum of the conductance curves starts to move towards higher potassium mole fractions at about 1,300°C which, however, is still within the temperature range of the measurements and disappears at 1,900°C, whereas the maximum of the activation energies is retained well above 2,000°C.

The results can be summarized in the following way. The mixed alkali effect of conductance and activation energy of conductance exists also in the molten state, which

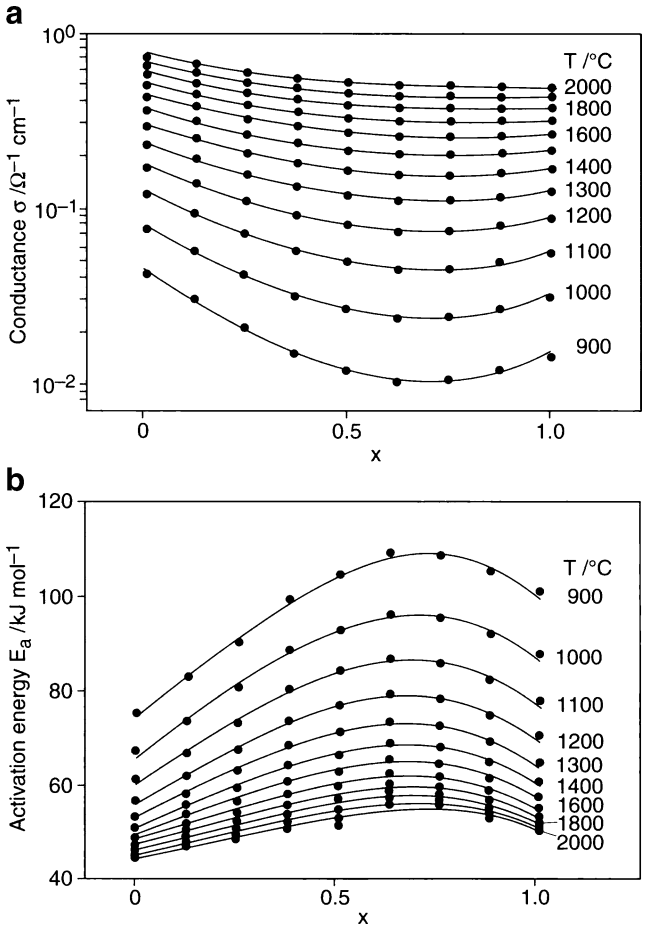

Fig. 10 **a** Conductance as a function of potassium mole fraction x of the mixed alkali glass system $(1-x)Na_2O \cdot xK_2O \cdot 0.7CaO \cdot 4.8SiO_2$ at various temperatures. **b** Activation energy of conductance as a function of potassium mole fraction x of the mixed alkali glass system as given in Fig. 10a at various temperatures

had not been shown for the activation energy before. That the effect of conductance does not "survive" above 1,900°C—different from that of the activation energy—may be explained by the extrapolation of the sensible conductivity data from 1,550°C to 2,000°C (see Fig. 10a). At any rate, the activation energy shows the mixed alkali effect clearly at and above 2,000°C. It is thus recommended to use activation energies instead of conductivities when the mixed alkali effect is studied in the future.

Spontaneous oxygen bubble formation at melt/refractory interfaces

Reaction mechanism The formation of gas bubbles during glass melting is a serious problem not only because of esthetic reasons, as in household glasses, and for functional reasons, as in optical glasses, but also because they can present considerable safety problems, for instance in television tubes and screens. Bubbles can be generated in glass melts by various causes, for instance, by the reboil of insufficiently fined glass melts [61, 62], by water vapor from defective cooling arrangements of glass melters, and by sodium chloride frequently used as fining agent, both of which can cause vacuum bubbles in glass products because water and salt vapors condense in the voids formed at melt temperatures on cooling the glass to ambient temperatures.

However, bubbles can also be formed by the mere contact of oxidic melts with refractories, which are used as building and lining materials of glass melting furnaces. The most interesting material is zirconium silicate (ZS), which has an especially long lifetime because of its high chemical resistivity to oxidic melts at high temperatures. The formation of bubbles at ZS is thus of high economical and scientific interest, and only two publications with proposed mechanisms had appeared when the Electrochemical Laboratory was asked in 1966 to investigate the reaction in detail. Neither paper, however, gave the cells employed for the investigations nor a detailed reaction mechanism [63, 64].

The ZS refractories used for the investigation at Schott Laboratory were ZS 1300 with the low apparent porosity of 0.5% and containing the impurities Fe_2O_3 (0.12 wt.%) and TiO_2 (1.28 wt.%), and ZS 834 dense with the apparent porosity of 2.9–3.4% and containing 0.08 wt.% Fe_2O_3 and 0. 25 wt.% TiO_2 [65]. Dissociation of these refractories into ZrO_2 and SiO_2 is restricted to high-temperature high-alkaline environments and was thus excluded during our experiments. The glass melts applied were alkali calcium silicates with 15.5 mol% alkali oxide (alkali=lithium, sodium, potassium, or sodium–potassium with a mole ratio 1:1), 10.8 mol% calcium oxide, and 73.7 mol% silicon dioxide and containing 0.2 wt.% Sb_2O_3 as a fining agent.

The work showed that the reaction is basically an oxidation of oxide ions of the melt at the melt surface by redox impurities, e.g., Fe_2O_3, which are frozen-in in a highly oxidized state at the high temperature of ZS fabrication [66]. The first step of this process is the formation of a phase boundary redox equilibrium between melt and refractory, Eq. 64,

$$2O^{2-}(s=0) + 4Fe^{3+}(s=0) \rightleftarrows O_2(s=0) + 4Fe^{2+}(s=0), \quad (64)$$

where s means distance from the interface melt/ZS. This equilibrium, however, is not maintained, because the reaction continues into the ZS and because of the too small oxygen amount formed at the two-dimensional melt/ZS interface.

The continuation of the reaction consists of five steps:

1. Oxidation of oxide ions at the ZS surface,

$$2O^{2-}(s=0) \rightarrow O_2(s=0) + 4e^{-}(s=0), \quad (65)$$

2. Transport of the liberated electrons from the ZS surface to the time-dependent depth $s(t)$ in the ZS,

$$4e^-(s=0) \rightarrow 4e^-(s(t)), \tag{66}$$

3. Consumption of the arriving electrons by the internal reduction of ferric ions,

$$4e^-(s(t)) + 4Fe^{3+}(s(t)) \rightarrow Fe^{2+}(s(t)), \tag{67}$$

4. Balance of the charge difference of the phases caused by the introduced electrons by a transfer of alkali ions from the melt into the solid,

$$M^+(\text{melt}, s=0) \rightarrow M^+(s=0), \tag{68}$$

and finally,

5. Transport of the alkali ions from the ZS surface to the site of the internal reduction of ferric ions,

$$M^+(s=0) \rightarrow M^+(s(t)). \tag{69}$$

$$2O^{2-}(s=0) + 4Fe^{3+}(s(t)) + 4M^+(\text{melt}, s=0) \rightarrow O_2(s=0) + 4Fe^{2+}(s(t)) + M^+(s(t)), \tag{70}$$

is the summary of the foregoing equations and describes the entire internal reaction. However, the transport of electrons and the steps of alkali ion transport, which have cancelled in this equation, must additionally be taken into account when kinetic viewpoints are to be considered. For instance, the reaction rate is seen to decrease with increasing reaction time. Schmalzried has thoroughly treated internal reactions in crystalline phases [67]. The reaction treated here, however, differs in that only traces of material react so that any phase changes are excluded.

The precondition for the reaction is a sharp boundary between the reduced and the original ZS, which was verified experimentally by IBSCA analysis. Besides, the step profile of the sharp boundary between the flesh-colored highly oxidized ZS and the light-gray reduced surface layers moved into the ZS during the reaction and slowed down with increasing distance from the interface. It was accompanied by an initially strong oxygen bubble formation, whose rate also decreased with time. This effect, incidentally, could often be repeated by grinding off the gray ZS layer and starting the reaction anew.

The reaction is unique indeed and is possible only because of the fortuitous combination of several properties of the materials: ZS is sufficiently electron- as well as cation-conducting at the oxidized and reduced state of the impurities, the impurity redox couple is present in a highly oxidized non-equilibrium state in the ZS, and melt and impurity of the ZS form a second redox couple in an appropriate energetic state. In addition, the high temperatures allow the cell reaction to take place at reasonable rates.

The internal reaction complex was investigated by means of a ZS specimen contacted at the (dry) rear side by an evaporated platinum layer and a zirconia and a platinum electrode present in the same silicate melt. This arrangement allowed short-circuiting the ZS with the other electrodes, measurement of equilibrium potentials of the ZS, and positive as well as negative polarization of the ZS specimen [68]. The experimental arrangement for these measurements is presented in Fig. 11 of this paper, and the results of all measurements are schematically summarized in Table 3.10 on pp. 400/401 of [1], which presents also the details of the measurements described.

The electrochromic character of the reaction The reaction between ZS and oxidic (or halide) melts is a type of electrochromic reaction. Figure 12 demonstrates this by comparing it with the electrochromic reaction of tungsten trioxide. Both processes involve an internal reduction, i.e., ferric to ferrous ions in ZS and tungsten trioxide to its bronze HWO_3 with partly reduced fivefold positive tungsten in WO_3. The corresponding reactions at the surfaces are the oxidation of oxide to oxygen at the ZS/melt interface and of hydrogen to hydrogen ions at the tungsten trioxide/platinum interface. Also, the electron transport from the locations of oxidation at the interfaces to those of the internal reduction and the charge-balancing alkali ion transport correspond to each other. The partly reduced materials are distinguished by coloration: The reduced ZS containing ferric and ferrous ions has a flesh-like color in contrast to the gray reduced ZS containing only ferrous ions and the dark blue tungsten bronze containing five- and sixfold tungsten in contrast to the nearly colorless tungsten trioxide. Both reactions can also be conducted in the field-driven mode, as demonstrated by Fig. 12. Here, the electrons are introduced into the solid by an electric field, which introduces also the charge-balancing cations, although from the opposite side of the solid. The internal reductions are principally the same in both cases. The reactions take place at vastly different temperatures. Their similarity is of no practical interest, but their comparison may nevertheless be of some interest with respect to the underlying reactions, particularly because the electrochromic or chromogenic reversible reaction

$$\text{colorless tungsten trioxide} \rightleftarrows \text{deep blue tungsten bronze}$$

is the basis of optically active thin layer systems, for instance of automotive rear view mirrors with continuously variable reflectivity [69].

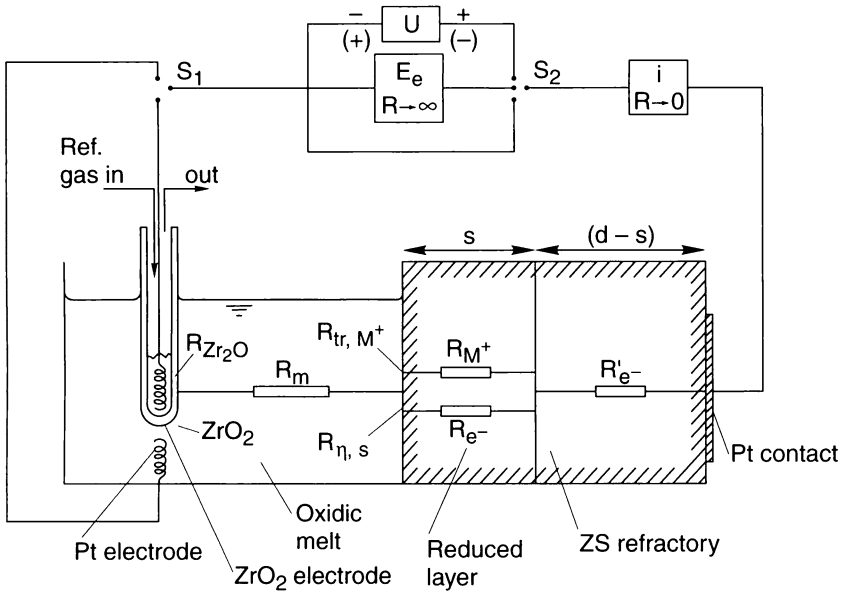

Fig. 11 Experimental arrangement for investigating the redox reaction between oxidic glass melts and redox impurity-containing ZS (internal reaction) offering (1) measurement of time-dependent cell voltage *E*e (*t*), (2) positive and negative polarization of ZS by external voltage *U*, and (3) short-circuiting of various cell combinations

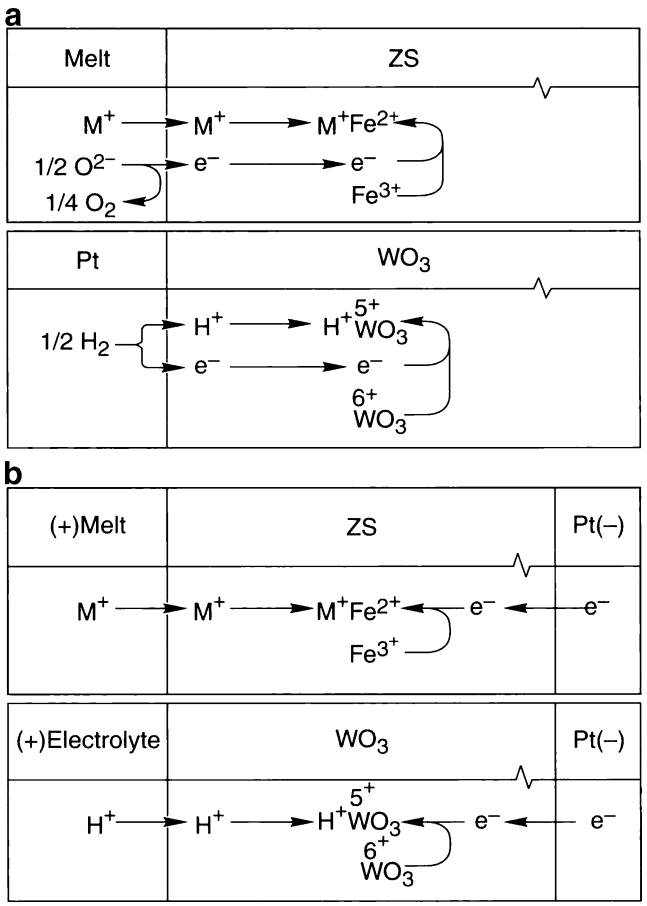

Fig. 12 Schematic demonstrating the electrochromic character of the redox reaction between oxidizable melts and redox impurity-containing ZS. **a** Spontaneous reactions and (**b**) field-driven reactions

Technical significance of the internal reaction The investigated reaction can have serious consequences with respect to oxygen bubble formation. As an example, the calculation reveals the following number of bubbles. Take 1 m^2 surface of a melting tank lined with ZS refractory that contains 0.1 wt.% iron, as an impurity of which, 10% are transferred from the oxidized to the reduced state within a layer thickness of 1 mm. This ZS surface area will produce 53,800 oxygen bubbles with 2 mm diameter or 430,600 oxygen bubbles with 1 mm diameter at 1,200°C, if the total of oxygen appears as bubbles or, respectively, 5.3 and 43.6 bubbles per minute and square meter tank surface if 7 days of the reaction with a constant reaction rate are assumed. This assumption is certainly unrealistic but, nevertheless, demonstrates impressively the effect of 100 ppm ferric ions referred to the 1-mm-thick refractory layer causing them and shows that a trace impurity can seriously disturb the economy and practical feasibility of a large-scale technical process as glass melting. Even more striking, the impurity (iron) is part of the reactor material and does not enter the product.

Electrolytic fining of glass melts

General As mentioned above, a common difficulty in glass melting is the formation of gas bubbles, for instance of sulfur dioxide, carbon dioxide, carbon monoxide, nitrogen oxides, and oxygen, which are formed by the reactions of the raw materials and get necessarily into the melt. As mentioned earlier in this paper, however, bubbles cannot be tolerated in glass products and must consequently be

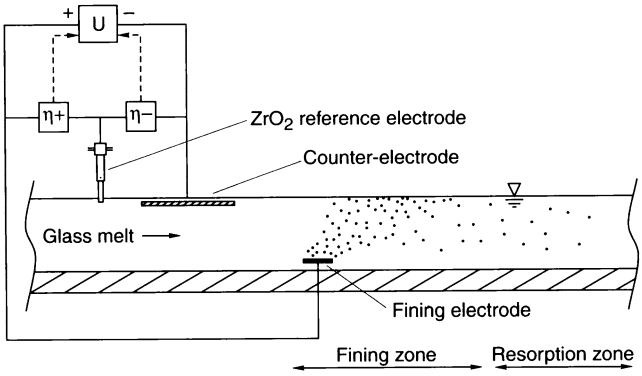

Fig. 13 Principle of electrolytic fining in a continuous melting furnace. The electrolyzing voltage U is controlled by a zirconia reference electrode, which keeps the anodic, η_+, and the cathodic polarization, η_-, within the "electrolytic window"

removed from the melt. Several processes have been developed, which remove such bubbles from glass melts. This procedure is called fining [70–76], the main process of which is adding small amounts of materials to the raw materials which, for instance due to a chemical reaction at high temperatures, form oxygen, which is dissolved in the melt and either diffuses into the impurity bubbles, blows them up so that they rise to the melt surface because of their increased buoyancy and leave the melt or, conversely, the oxygen forms blisters, into which the impurity gases diffuse so that their volume increases and, due to their increased buoyancy, rise to the melt surface and also leave the melt.

However, there are not many substances available which react in the desired and harmless way, and if they do, they are more or less hazardous to the environment. Thus, arsenic oxide has already been banned from glass melting, and even small amounts of antimony oxide will be excluded as soon as (and if) an economically more tolerable fining agent has been found.

The electrolytic fining procedure A discussion of feasible solutions to this problem at Schott Laboratory in the late 1980s resulted in the proposal of *electrolytic fining* [77], a process which has meanwhile been patented [78]. It is based on oxygen as the fining gas. Different from redox fining, however, the oxygen bubbles are not generated by a temperature-dependent dissociation of oxides but by a physical process, i.e., by an electrolysis of the oxidic glass melt. The use of fining agents is thus nearly eliminated from the fining step and is reduced to small amounts, which are needed to remove stray oxygen blisters from the quiet or resorption zone, which the melt subsequently enters. The necessary amount of fining agent needed is consequently drastically reduced and, in addition, is strongly dependent on the conditions of the resorption zone, for example, by the number and size of oxygen blisters of the melt entering the quiet zone and the temperature profile and residence time of the melt in the resorption zone. The process is thus externally controllable.

Technical arrangement of electrolytic fining The melting tank with the active parts of the electrolysis constitutes a relatively long electrolytic trough, through which the glass melt flows in a possibly thin layer, after it has left the raw melt section of the melter (Fig. 13). The fining anode is located near the bottom and as far away from the outlet of the furnace as feasible so that the rest of the blisters is kept at a low level. The counter cathode positioned upstream or in a by-pass, from which small parts of the melt are discarded is constructed so as to reduce as much oxygen to oxide as possible without necessitating too high overpotentials (e.g., by a large surface area, closeness to the melt surface, movement relative to the melt, or bubbling with oxygen).

An important part of the arrangement is the control part, which protects particularly the platinum cathode. Platinum can be oxidized as well as "reduced," especially in glass melts containing easily reducible elements, which amalgamate with platinum and can thus destroy platinum parts at the

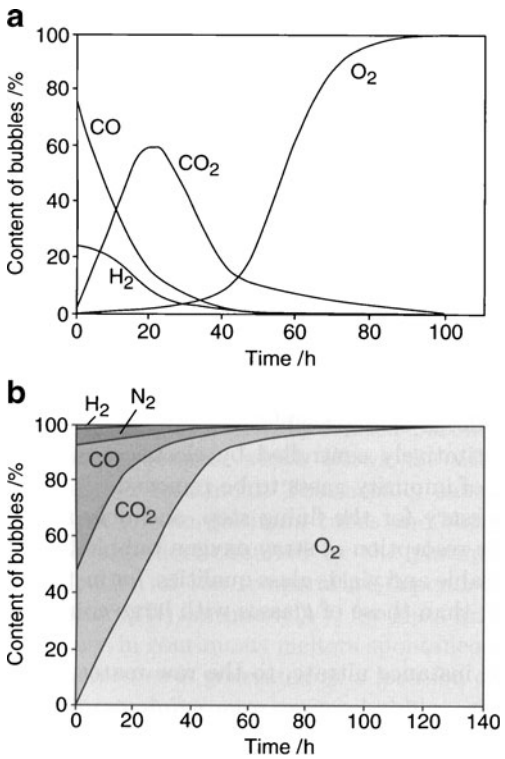

Fig. 14 Time-dependent composition of gas bubbles during a test of laboratory electrolytic fining of a sodium calcium silicate melt without fining agent at 1,300°C. **a** Strongly reducing melt containing carbon monoxide and hydrogen. Only gas contents of special interest are plotted, the rest being nitrogen and water (not measured). **b** Weakly reducing melt containing equal amounts of carbon monoxide and carbon dioxide, less nitrogen and a trace of hydrogen (integral curves)

high temperatures of glass melting. The applied voltages are thus protected by maximum values, which are determined by means of reference electrodes, for example, zirconia electrodes, as shown in Fig. 13. The necessary electrochemical data can easily be obtained from current–voltage curves measured at practically relevant temperatures. Actual data cannot be given in this paper but must be obtained by practical measurements under appropriate conditions.

Test application in a laboratory The basic feasibility of *electrolytic fining* has been shown by laboratory measurements, where a sodium calcium silicate melt could nearly completely be freed of CO, CO_2, N_2, and H_2 in a special crucible (see Fig. 14). The experiments have shown that much development work is still needed for a technical application of the principle, which may even include the construction of a special kind of melter. However, the environmental requirements of the future may not give many other possibilities a chance.

Conclusion

This paper has reported some of the work that has mostly been carried out in addition to the work that had to be done as the task of an electrochemical laboratory of the glass industry. The text has become rather extended because most of the material could not be expected to be well known to the readers (especially outside the glass industry), although a certain number of references has been supplied. However, some subjects had to be omitted because of the already extended length of the paper, although the author would have liked to report on them.

The following subjects, which have already been treated, were omitted but can be found in the cited book [1].

- Comparison of glass and ion exchanger electrodes,
- A thorough discussion of the thermodynamic hypotheses by Nicolsky and Eisenman, as far as they have not been covered in this paper, which have often erroneously been called theories of the glass electrode,
- The relationship of silicate and borate electrolyses, which exhibit quite different features,
- The basis of pH measurements, which the author had the chance to be involved in as a member of the Interdivisionary Working Party on pH of IUPAC,
- The optical basicity of glass-forming melts with J.A. Duffy,
- Diagram of the oxidation state of glass melts (short-circuited metals in non-isothermal melts),
- Electrochemical displacement of disturbing reactions, e.g., oxygen bubble formation, from critical places to harmless locations in glass melters, and
- Thin layer systems with changeable optical constants, e.g., automotive rear view mirrors with continuously variable reflectivities.

This material may suffice to write an additional volume on *Fundamental and Applied Electrochemistry at an Industrial Glass Laboratory*, which may be an interesting task in the future.

References

1. Bach H, Baucke F, Krause D (eds) (2000) Electrochemistry of glasses and glass melts, including glass electrodes, Schott series on glass and glass ceramics, science, technology, and applications. Springer, Berlin
2. Schwabe K, Suschke D (1964) Angew Chem 76(1):39–49
3. Haber F, Klemensiewicz F (1909) Z Phys Chem 67:385
4. Haber F (1908) Ann Phys 26:927
5. Lengyel BV. Z Phys Chem Abt A 153:425 (1931), 159:145 (1932), 159:393 (1932)
6. Cremer M (1924) Beitr Physiol 2:229
7. Cremer M (1906) Z Biol 47:562
8. Schwabe K, Dahms H (1960) Isotopentechnik 1:3439
9. Nicolsky BP (1937) Acta Physicochim USSR VII:597
10. Schiller H (1924) Ann Phys 74:105
11. Horovitz K, Zimmermann J (1925) Sitzungsber Akad Wiss Wien Abt IIa 134:355
12. Eisenman G (ed) (1967) The origin of the glass electrode potential. Glass electrodes for hydrogen and other cations, principles and practice. Dekker, New York, vol. 5, pp 133–173
13. Baucke FGK (1996) Ber Bunsenges Phys Chem 100(9):1466f
14. Bach H, Baucke FGK (1982) J Am Ceram Soc 65:527
15. Bouquet G, Dobos S, Boksay Z (1964) Ann Univ Sci Bp Rolando Eötvös Nomin Sect Chim 6:5
16. Robinson RA, Stokes HH (1968) Electrolyte solutions, 2nd edn. Butterworths, London, pp 104–109
17. Baucke FGK (2001) Phys Chem Glasses 42(3):220
18. Baucke FGK (1974) J Non-cryst Solids 14:13
19. Baucke FGK (1975) J Non-cryst Solids 19:75
20. Bard AJ, Inzelt G, Scholz F (eds) (2008) Electrochemical dictionary. Springer, Berlin, p 306
21. Baucke FGK (1994) Anal Chem 66:4519
22. Baucke FGK (2001) Phys Chem Glasses 42(3):200
23. Bates RG (1973) Determination of pH: theory and practice, 2nd edn. Wiley, New York, pp 440–443
24. Baucke FGK (2001) Phys Chem Glasses 42(3):222
25. Baucke FGK (1994) Anal Chem 66:4522
26. Baucke FGK (2009) Chem Anal (Warsaw) 54:1117
27. Covington AK, Paabo M, Robinson RA, Bates RG (1968) Anal Chem 40:700–706
28. Gary R, Bates RG (1964) J Phys Chem 69:1–7
29. Baucke FGK (1998) J Phys Chem B 102:4835–4841
30. Glasoe PK, Long FA (1960) J Phys Chem 64:188–191
31. Baucke FGK, Naumann R, Alexander-Weber C (1993) Anal Chem 65:3244–3251
32. Gary R, Bates RG, Robinson RA (1964) J Phys Chem 68:3806–3809
33. Eisenman G (1967) The physical basis for the ionic specificity of the glass electrode. In: Eisenman G (ed) Glass electrodes for hydrogen and other cations, principles and practice. Decker, New York
34. Lowe BM, Smith DG (1973) Anal Lett 6:903–907

35. Lowe RM, Smith DG (1974) Electroanal Chem Interfacial Eletrochem 51:295–303
36. Jorgensen PJ, Norton FJ (1969) Phys Chem Glasses 10:23–27
37. Bazán JC (1978) Z Phys Chem NF 110:285–288
38. Perley GA (1948) US Patent No. 2 444 845
39. Perley GA (1949) Anal Chem 21:394–401
40. Baucke FGK (1994) J Electroanal Chem 367:134–139
41. Martell AE, Smith HM (eds) (1976) Critical stability constants, Vol. 4. Inorganic complexes. Plenum, New York, p 56
42. Tananaev IV, Rozanov IA, Beresnev EN (1996) Izv Akad Nauk SSSR Neor Mater 5:419–426 (English translation: 347-553)
43. Mooney RCI (1948) J Chem Phys 16:1003
44. Mooney RCI (1950) Acta Crystallogr 3:337–340
45. Eisenman G (1967) The origin of the glass electrode potential. In: Eisenman G (ed) Glass electrodes for hydrogen and other cations. Dekker, New York, pp 133–173
46. Cable M (1984) Principles of glass melting. In: Uhlman DR, Kreidl NJ (eds) Glass science and technology, vol 2. Academic, Orlando, pp 1–44
47. Reuther H, Wiegmann J, Hinz W (1983) Part 1, Glastechn Ber 56:19–25, Part 2, Glastechn Ber 56:47–50 (1983)
48. Oldekop W (1956) Glastech Ber 29:73–78
49. Carlson DE, Trzeciak CE (1973) Phys Chem Glasses 14:10–15
50. Baucke FGK, Mücke K (1986) J Non-Cryst Solids 84:174–182
51. Baucke FGK, Frank WA (1976) Glastech Ber 49:157–161
52. Kropp S (1980) Diploma Thesis. FH Fresenius, Wiesbaden
53. Baucke FGK, Braun J, Röth G, Werner R-D (1989) Glastech Ber 62:122–126
54. Swenson O (1980) Glastek Tidskr 35(1):5–11
55. Th Pfeiffer, Müller R, Werner R-D (1996) Phys Chem 100:1503–1507
56. Isard JO (1969) J Non-Cryst Solids 1:235–261
57. Day DE (1976) J Non-Cryst Solids 21:343–372
58. Kostanyan KA (1960) Investigation of the conductivity neutralization effect in fused borate glasses. In: The structure of glass, Vol. 2, Proc. Third All-Union Conf. on the Glassy State, Leningrad, 1959. Consultants Bureau, New York, pp 234–236
59. Tickle RE (1967) Phys Chem Glasses 8:101–112
60. Tickle RE (1967) Phys Chem Glasses 8:113–124
61. Baucke FGK, Pfeiffer T (Oct. 1993) German Patent 4 207 059
62. Baucke FGK (1987) Solar Energy Mat 16:67–77
63. Bossard AG, Begley ER (1966) In: Symposium on defects in glass. Ann. Meeting ICG. Tokyo, Kyoto, pp 69–81
64. Bedros P, Fojtková M (1984) Sklár Keram (Orig Czech) 34:349–352
65. Corhart Refractories, Ceramic Products Div., Corning Glass Works (USA) (1985) Corhart® ZS dense zircon refractory. In: Fiberglass and specialty refractories, pp. 1.00ff., 1.01ff
66. Baucke FGK, Röth G (1988) Glastech Ber 61:100–118
67. Schmalzried H (1995) Chemical kinetics of solids. VCH, Weinheim, pp 209–233
68. Baucke FGK, Röth G (1992) German Patent 41 09 652
69. Bedroš P, Štveràk J (1985) Sklàr Keram 35:142–143
70. Cable M, Frade JR (1987) Glastech Ber 60:355–362
71. Yoshikawa H, Kawase Y (1997) Glastechn Ber Glass Sci Technol 70:32–40
72. Hübenthal H, Frischat GH (1987) Glastech Ber 60:1–10
73. Beerkens RGC (1990) Glastech Ber 63K:222–242
74. Cable M (1984) Principles of glass melting. In: Uhlmann DR, Kreidl NJ (eds) Glass science and technology, Vol. 2. Processing. Akademic Press, Orlando, pp 16–28, Chap. 1
75. Krüger F (1938) Glastech Ber 16:233–236
76. Eden C (1952) Glastech Ber 25:83–86
77. Baucke FGK (1992) Laboratory Report 60/92. Schott Glas, Mainz
78. Baucke FGK, Pfeiffer T (Oct. 1993) German Patent 42 07 059
79. Swenson O (1980) Part II, Glastek Tidskr 35(2):37–40